FATIGUE CRACKING OF RIVETED, COPED, STRINGER-TO-FLOORBEAM CONNECTIONS

WA-RD 494.1

Final Report
March 2001

Washington State Department of Transportation

Washington State Transportation Commission
Planning and Programming Service Center
in cooperation with the U.S. Department of Transportation
Federal Highway Administration

Research Report
Research Project T9903, Task 98
Bridge Fatigue Repair

FATIGUE CRACKING OF RIVETED, COPED, STRINGER-TO-FLOORBEAM CONNECTIONS

by

Charles W. Roeder
Professor

Gregory A. MacRae
Assistant Professor

Athena Y. Kalogiros
Research Assistant

Amy Leland
Research Assistant

Department of Civil and Envinronmental Engineering
University of Washington, Box 352700
Seattle, Washington 98195-2700

Washington State Transportation Center (TRAC)
University of Washington, Box 354802
1107 NE 45th Street, Suite 535
Seattle, Washington 98105-4631

Washington State Department of Transportation
Technical Monitor
Harvey Coffman
Bridge Preservation Engineer, Bridge and Structures

Prepared for
Washington State Transportation Commission
Department of Transportation
and in cooperation with
U.S. Department of Transportation
Federal Highway Administration

March 2001

TECHNICAL REPORT STANDARD TITLE PAGE

1. REPORT NO.	2. GOVERNMENT ACCESSION NO.	3. RECIPIENT'S CATALOG NO.
WA-RD 494.1		

4. TITLE AND SUBTITLE	5. REPORT DATE
Fatigue Cracking of Riveted, Coped, Stringer-to-Floorbeam Connections	March 2001
	6. PERFORMING ORGANIZATION CODE
7. AUTHOR(S)	8. PERFORMING ORGANIZATION REPORT NO.
Charles W. Roeder, Gregory A. MacRae, Athena Y. Kalogiros, Amy Leland	
9. PERFORMING ORGANIZATION NAME AND ADDRESS	10. WORK UNIT NO.
Washington State Transportation Center (TRAC) University of Washington, Box 354802 University District Building; 1107 NE 45th Street, Suite 535 Seattle, Washington 98105-4631	11. CONTRACT OR GRANT NO. Agreement T9903, Task 98
12. SPONSORING AGENCY NAME AND ADDRESS	13. TYPE OF REPORT AND PERIOD COVERED
Research Office Washington State Department of Transportation Transportation Building, MS 47370 Olympia, Washington 98504-7370 Keith Anderson, Project Manager, 360-709-5405	Research report
	14. SPONSORING AGENCY CODE

15. SUPPLEMENTARY NOTES

This study was conducted in cooperation with the U.S. Department of Transportation, Federal Highway Administration.

16. ABSTRACT

Fatigue cracking has been noted in a number of riveted, coped stringer-to-floorbeam connections on truss bridges in Washington state. The fatigue cracking has raised uncertainty regarding the future performance and life expectancy of these bridges. This laboratory experimental research study evaluated the expected performance of these critical connections to better understand the causes of the fatigue cracking and to compare and evaluate several damage limitation methods for this critical location.

Sixteen test specimens were built and tested. During the initial testing, the goal was to develop fatigue cracks in the region of the cope. The cracks were observed, and the rate of crack growth was closely monitored. The results of this work showed that the rate of initial visible cracking is dependent on the surface condition of the cope. Rough or notched copes develop cracks after a very few cycles. Once the crack has developed, the rate of crack growth does not depend on the surface condition of the cope.

A damage limitation method (DLM) was applied to most specimens. Three methods—the hole drilling method, the drilled hole with inserted bolted, and the bolt removal method—were evaluated. After the DLM was applied, the specimen was retested to determine whether and when further crack growth occurred. The rate of crack growth was closely monitored, and the relative effectiveness of alternative DLMs were determined.

A design and evaluation procedure was developed for predicting the time required for crack development and for selecting appropriate connection stiffnesses for application of the DLMs. This method utilizes load spectra developed in previous field investigations and methods for translating the load spectra into an effective stress and number of cycles for the fatigue evaluation. Models are provided for evaluating connection stiffness and for analyzing the effect of the connection stiffness on the stringer moments.

17. KEY WORDS	18. DISTRIBUTION STATEMENT
Coped stringers, damage limitation, fatigue, fatigue cracking, fatigue life, repair, riveted connections	No restrictions. This document is available to the public through the National Technical Information Service, Springfield, VA 22616

19. SECURITY CLASSIF. (of this report)	20. SECURITY CLASSIF. (of this page)	21. NO. OF PAGES	22. PRICE
None	None		

DISCLAIMER

The contents of this report reflect the views of the authors, who are responsible for the facts and the accuracy of the data presented herein. The contents do not necessarily reflect the official views or policies of the Washington State Transportation Commission, Department of Transportation, or the Federal Highway Administration. This report does not constitute a standard, specification, or regulation.

CONTENTS

FIGURES

TABLES

SUMMARY
FATIGUE CRACKING OF RIVETED, COPED STRINGER-TO-FLOORBEAM CONNECTIONS

Fatigue cracking has been noted in a number of riveted, coped stringer-to-floorbeam connections on truss bridges in Washington state. These bridges are mainly on Interstate highways and other heavily used routes, and they are critical to the economy and transportation system of the state. The fatigue cracking has raised uncertainty regarding the future performance and life expectancy of these bridges. This laboratory experimental research study evaluated the expected performance of these critical connections to better understand the causes of the fatigue cracking and to compare and evaluate several damage limitation methods for this critical location.

Sixteen test specimens were built and tested. During the initial testing, the goal was develop fatigue cracks in the region of the cope. The cracks were observed, and the rate of crack growth was closely monitored. Several specimens were tested until cracks had developed to a very large size and the specimen was beyond effective repair. However, a damage limitation method (DLM) was applied to most specimens. Three methods—the hole drilling method, the drilled hole with inserted bolted, and the bolt removal method—were evaluated. After the DLM was applied, the specimen was retested to determine whether and when further crack growth occurred. The rate of crack growth was closely monitored, and the relative effectiveness of alternative DLMs were determined.

The results of this work showed that the rate of initial visible cracking is dependent on the surface condition of the cope. Rough or notched copes develop cracks

after a very few cycles, whereas flame cut copes with a reasonable surface finish may require a number of cycles an order of magnitude higher to develop the initial visible crack. Once the crack has developed, the rate of crack growth does not depend upon the surface condition of the cope.

The drilled hole DLM delayed crack growth somewhat, but it did not return the specimen to anything approaching an undamaged state. Cracks developed more quickly with this method than with undamaged specimens that had a good initial cope finish. The drilled hole with inserted bolt was very effective at retarding further crack growth, since it delayed re-initiation of crack growth for a period of time that was comparable to the period required for initiation of cracks in a smooth cope detail. The bolt removal method was also very effective at retarding further crack growth if the connection stiffness was reduced to an appropriate value.

A design and evaluation procedure was developed for predicting the time required for crack development and for selecting appropriate connection stiffnesses for application of the DLMs. This method utilizes load spectra developed in previous field investigations and methods for translating the load spectra into an effective stress and number of cycles for the fatigue evaluation. Models are provided for evaluating connection stiffness and for analyzing the effect of the connection stiffness on the stringer moments.

INTRODUCTION

STATEMENT OF THE PROBLEM

WSDOT has more than 150 steel truss bridges with deck framing, as shown in Figure 1. Coped stringer-to-floorbeam connections are used, because the top flange elevations are similar for both the longitudinal stringers and transverse floorbeams. Web-angle connections, as illustrated in Figure 2a, are used at most interior joints, but stiffened-seat connections, as illustrated in Figure 2b, are used at joints with limited movement requirements. Most of these bridges were built before 1970, and they employ riveted connections. Riveted construction is not normally regarded as sensitive to fatigue, but significant fatigue cracking has been observed, as illustrated in Figure 3.

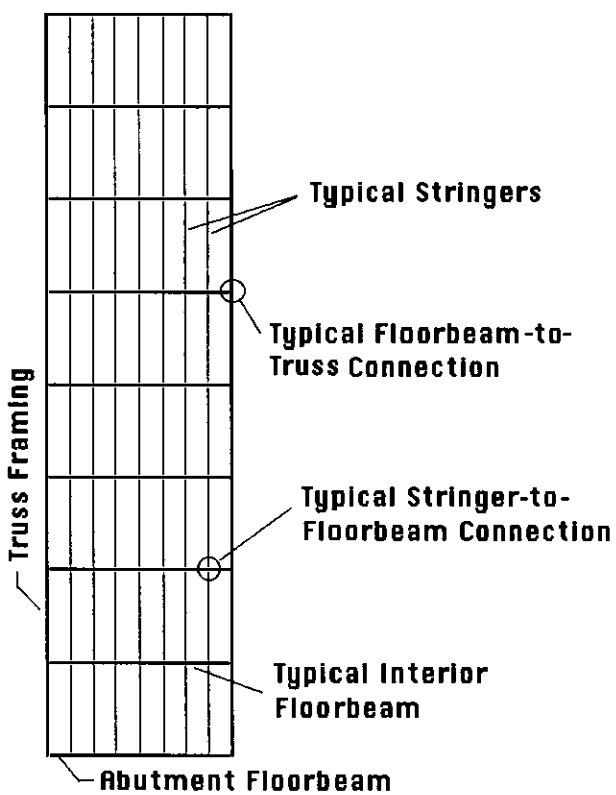

Figure 1. Typical Layout of Structural System for the Deck of Steel Truss Bridges

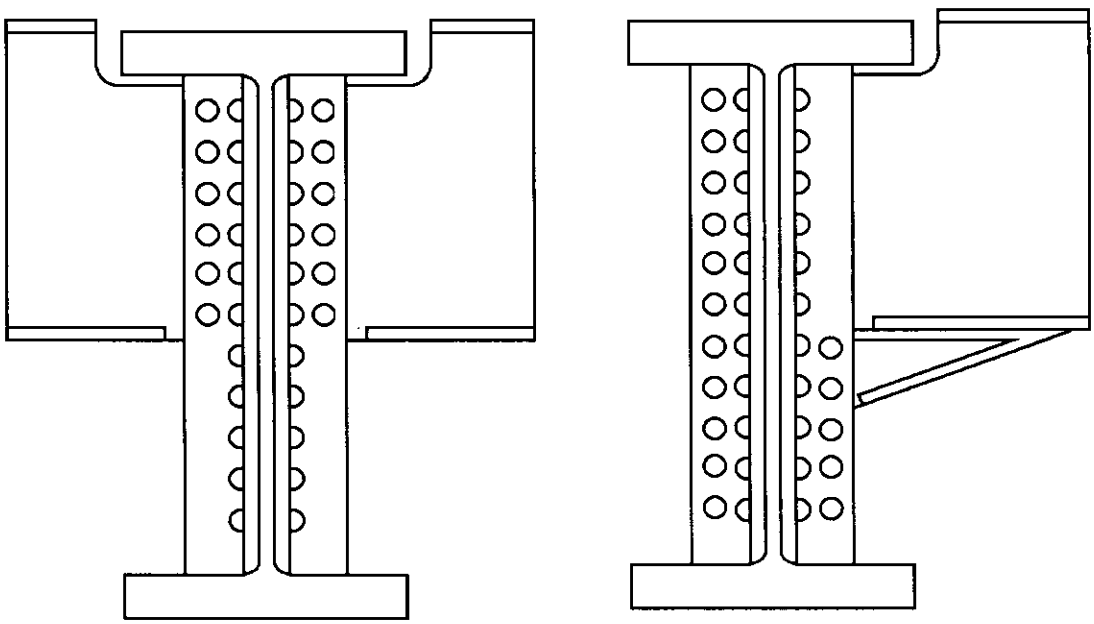

a) Coped Web Angle Connection b) Stiffened Seat Connection

Figure 2. Typical Stringer to Floor Beam Connections.

Figure 3. Photograph of Crack Starting and Stringer Cope and Progressing into Web

Fatigue cracks have occurred at the coped stringer-to-floorbeam connections of nearly all of these truss bridges. Southbound Interstate 5 across the Lewis River is a 3-span, continuous steel truss bridge, as illustrated in Figure 4, and Figure 5 shows the fatigue crack locations observed on this typical bridge. There is extensive cracking in a relatively large number of bridges, and this has raised serious questions regarding the remaining fatigue life and the repair and retrofit of these damaged steel truss bridges.

Figure 4. Photograph of the Lewis River Bridge

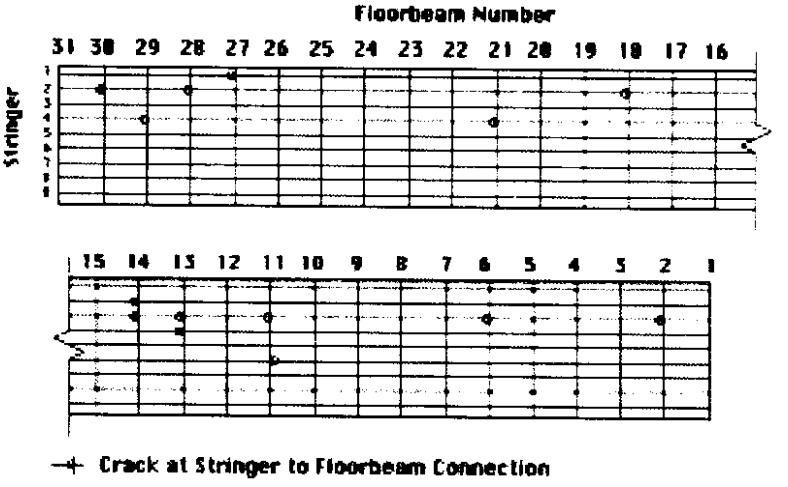

Figure 5. Locations of Cracking on the Lewis River Bridge

WSDOT engineers have used three damage limitation methods (DLMs) at these cracked locations. These methods are illustrated in Figure 6. For cracks that are shorter than 75 mm (3 inches), a 25-mm (1-inch) hole is drilled through the tip of the crack, as illustrated in Figure 6a, and the hole is polished to achieve an acceptable finish. Since this hole drilling method is intended to eliminate the tip of the crack, and the source of further crack growth, the tip of the crack must be accurately located. With some short cracks, a second method, the bolted DLM, is used. With this method, the 25-mm (1-inch) hole is drilled, and a 22-mm ($^7/_8$-inch) high strength bolt is inserted into the hole and tightened to develop its proof load, as illustrated in Figure 6b. The tensile force in the bolt induces a clamping force, which develops compressive stresses in the steel surrounding the hole and former crack tip location. Some compressive stresses are believed to be normal to the crack tip because of the lateral strains caused by Poisson's ratio and the confinement of the surrounding steel. Thus, the bolted DLM is intended to eliminate the tip of the crack and the source of crack growth, but the compressive stress is expected to further reduce the potential for crack growth.

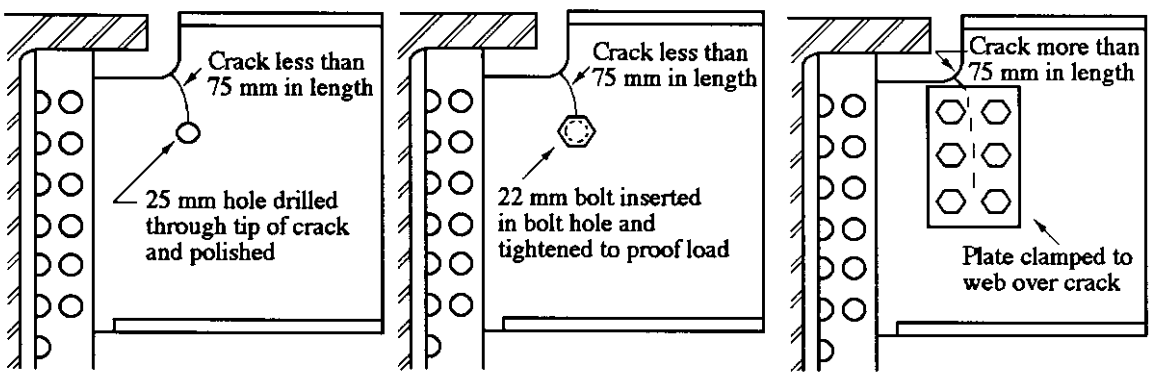

a) Hole Drilling DLM b) Bolted DLM c) Fishplate DLM

Figure 6. Damage Limitation Methods (DLM) Used by WSDOT Engineers

The third DLM, the fishplate DLM, utilizes a plate bolted to the web over the cracked area, as illustrated in Figure 6c, and is employed with longer cracks (cracks longer

than 75 mm or 3 inches). The clamping force of the bolts develops compressive stress in the region around the crack tip to deter further crack growth. In addition, the plate reinforces the web and reduces the stress in the steel in the critical region. The fishplate DLM is more difficult to employ, since it requires access to the crack over a significant area, and this is not always possible with the riveted stringer connection.

The above DLMs have been used, but with mixed success. In some cases, each of these repairs has been successful in controlling and preventing further crack growth, but in other cases, the methods were unsuccessful because significant crack growth was observed shortly after the DLM was employed. In addition, other possible DLMs have been considered but not yet employed.

RESEARCH OBJECTIVES

As noted earlier, WSDOT has a number of steel truss bridges. These bridges usually are part of major state highways or the interstate system, and they are important to the state and its economy. In recent years, cracking has been noted at riveted, coped stringer-to-floorbeam connections on most of these bridges, and the remaining fatigue life of these bridges is uncertain. The DLMs have had mixed success in controlling crack growth. However, damage limitation is essential because it is very costly to replace these bridges. As a result, this study was started to find a solution to this cracking issue. The research specifically focused on fatigue cracking in the coped stringer connections, as illustrated in figures 2 and 3. The specific objectives of the study were as follows:

- to better understand the fatigue cracking behavior, including determination of S-N curves that are appropriate for estimating the fatigue life prior to initial cracking
- to better estimate the rate of crack growth and the time required for serious structural problems to occur after cracking has begun
- to evaluate the effectiveness of different economical DLMs in controlling or preventing future crack growth

- to combine the laboratory testing completed in this study with the field testing completed during earlier work [Roeder et al 1998] to develop a comprehensive understanding of the cracking problem
- to develop design models for estimating the remaining fatigue life for these riveted, coped stringer connections and the application of DLMs to these connections.

BACKGROUND AND LITERATURE REVIEW

Riveted stringer connections are the focus of this research report. Fatigue was not considered in the initial design of these bridges because AASHTO fatigue design requirements were not developed until about 1974 [AASHTO 1973, Fisher et al 1970], and these riveted truss bridges were designed and constructed before this time. Furthermore, the initial AASHTO fatigue design requirements focused on welded connections [Fisher et al 1970, Schilling et al 1978]. The fatigue procedure that has evolved in the United States uses the S-N curves illustrated in Figure 7 and various categories of details to match the S-N curve to specific applications.

Category A reflects the fatigue life behavior for base metal with no holes, attachments, or section changes, and this curve permits relatively large stress ranges as a function of the number of cycles applied to the element. Increasing section changes are noted for elements as the stress range category progresses from A to E, E' or F, and significantly decreasing stress ranges are permitted for these more critical stress categories. The category assignments are based on the behavior observed in experiments from fatigue tests. The assignments are made through graphical representations of the loading and the connection detail. Most category assignments focus on welded structural details, and no categories are specifically assigned for riveted connections or for the coped stringer connection illustrated in Figure 2. Furthermore, the AASHTO fatigue categories were developed on the basis of observation of a visible crack approximately 25 mm (1 inch) long, and the S-N curves are defined to be approximately 2 standard deviations below the

mean. Therefore, only a small percentage of elements are expected to develop cracking at the specific number of cycles and the stress range defined by their appropriate S-N curve.

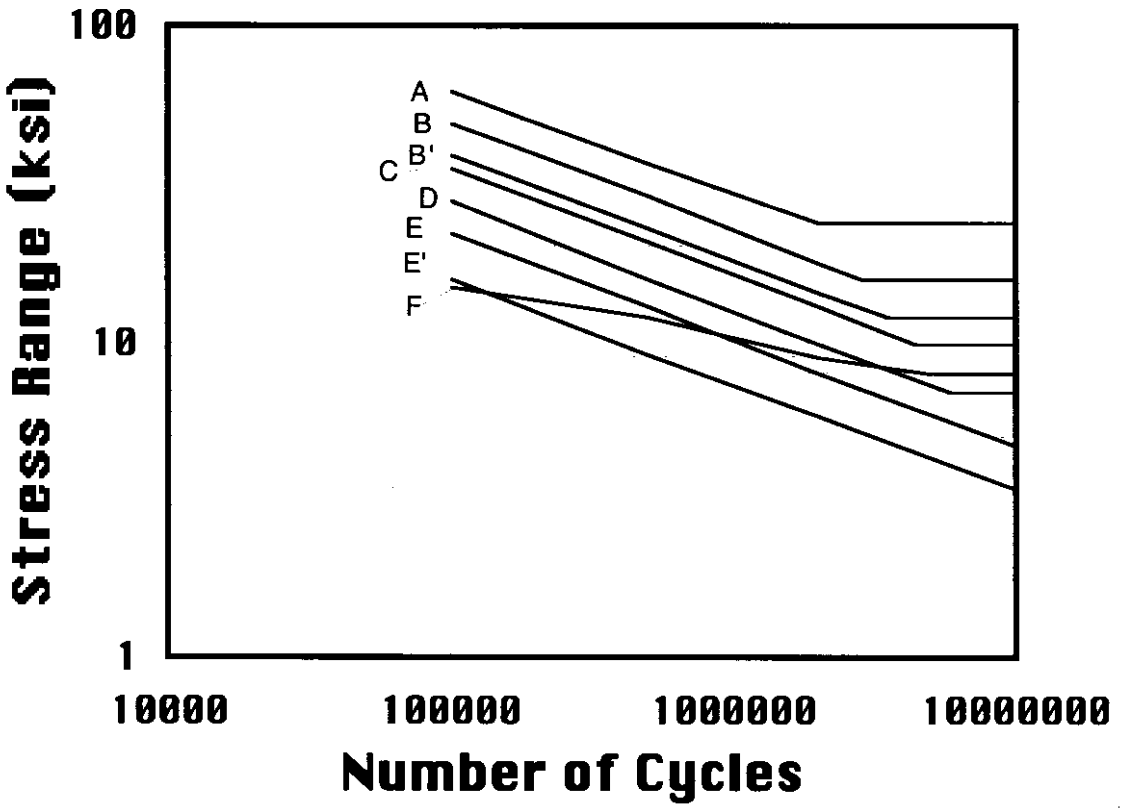

Figure 7. S-N Curves as Commonly Used in AASHTO Specifications

Fatigue design of bridges has historically been based upon 2 million cycles of the HS20 truckload. Engineers recognize that bridges will experience far more than 2 million stress cycles during their service life, but the stress range for the vast majority of these stress cycles will be smaller than the nominal design stress value. The bridge is actually subject to hundreds of millions or billions of variable amplitude stress cycles during its full service life. As a result, variable amplitude fatigue [Schilling et al 1978] is an issue of importance, and variations of Miner's rule [Miner 1945] are used to estimate the fatigue life for realistic stress and load conditions. This more realistic evaluation is normally required for fatigue life evaluation of existing bridges [Moses et al 1987, AASHTO 1990]. Miner's rule models cracking under accumulated damage by

$$\sum \left(\frac{n_i}{N_i}\right)^{\alpha} = 1 \qquad \text{(Eq. 1)}$$

where n_i is the number of cycles at a given stress level, N_i is the number of cycles that can be tolerated at that given stress level, and α is a coefficient used to represent the severity of the accummulation effect. The coefficient, α, is commonly used as 1.0 for fatigue problems. The slope of the log-log plot for S-N curves is a negative $\frac{1}{3}$, as illustrated in Figure 7, and so the Miner's rule for accumulation of variable amplitude fatigue damage is sometimes [Moses et al 1987] expressed as an effective constant stress range, σ_{eff}, where

$$\sigma_{eff} = \sqrt[3]{\frac{\Sigma n_i \sigma_i^3}{N}}. \qquad \text{(Eq. 2)}$$

This effective stress range can be applied to the S-N curves of Figure 7 with the same result as obtained with direct application of Equation 1, where σ_i is the given stress range, and N is the summation of n_i for all stress cycles.

The AASHTO LRFD design provisions [AASHTO 1994] are different yet similar to the historic standard specifications. The S-N curves are the same for both the standard specifications and LRFD specifications. However, the fatigue design loads and the load factors used for those loads are more rationally selected to provide an accurate estimate of the bridge fatigue life. The average daily truck traffic is estimated for the bridge, and the estimated number of load cycles for each lane of traffic is established by applying lane distribution factors to the average daily truck traffic. The standard truck loads for fatigue design in the LRFD specification are similar to those used in the standard specifications. However, this truck load is increased for impact and then multiplied by a load factor of 0.75 in recognition of the fact that the vast majority of the trucks crossing a bridge are

much lighter than the standard design vehicle. The resulting procedure leads to designs similar to those obtained with the standard specifications, but it more rationally considers the actual number of cycles and the load level achieved during those cycles than do the standard specifications. Furthermore, this LRFD procedure usually results in a much larger number of truck load cycles than that used with the standard specification.

Fatigue evaluation has advanced greatly in recent years, but there are serious limitations in evaluating the fatigue life of riveted, coped stringer connections. In general, riveted structures are not regarded as sensitive to fatigue, and few fatigue tests on riveted structures have been performed. A limited series of fatigue tests on built-up, riveted members [Fisher et al 1987] have been performed. These tests suggest fatigue Category D is a lower bound indicator of the initiation of cracking, and Category C is a lower bound indicator of the total fatigue life.

Coped beams with bolted connections have been tested [Yam and Cheng 1990], and these tests showed that fatigue cracking initiates from the cope of the beam section. In normal fatigue design calculations, nominal stresses are computed and compared to the S-N curves. However, the Yam and Cheng method for addressing coped connection fatigue requires that the stress concentration at the cope be estimated, because the stress concentration and the rates of crack initiation and crack growth are highly dependent on cope geometry. When this stress concentration was estimated, Category C was recommended as the best indicator of initiation of cracking and Category B was established as the better indicator of fatigue life.

Coped diaphragm connections were also tested [Zwernemann et al 1993]. This study recommended that Category D S-N curves be used to estimate fatigue cracking, but this method employed nominal stresses rather than the estimated stress concentrations employed by Yam and Chen. Together, these studies clearly show that fatigue cracks occur more quickly when

- the radius of the cope is small

- or when the surface finish of the cope is rough.

However, they also show that there is uncertainty regarding the fatigue category that should be applied to this detail.

Another recent study [Roeder et al. 1998, Wong 1997] included field measurements of riveted truss bridges. The field measurements showed the load spectrum developed on the Lewis River Bridge, and the study evaluated the causes of fatigue cracking on the bridge. The study showed that riveted, coped stringer-to-floorbeam connections develop significant rotational restraint, although the connections were originally designed as pinned connections. The rotational restraint causes significant negative bending moments in the region of the cope, and the negative bending moment induces tensile stresses at the top of the beam at the cope. The stringer copes on the older truss bridges often had very rough flame cut surfaces, because no consideration was given to fatigue during their construction. Past research has shown that this rough cutting of the cope, combined with the tensile stress induced by the moments because of the rotational restraint, causes the stress range that leads to fatigue cracking.

The importance of the connection stiffness raises the possibility of another DLM, as illustrated in Figure 8. The connection stiffness [Roeder 2000] depends upon the number of rivets (or bolts) in the connection, and therefore one economical repair method may be to reduce the number of these bolts or rivets. A reduction in the number of connectors would reduce the connection stiffness, and this would reduce the negative bending moment and the stress range in the region of crack development.

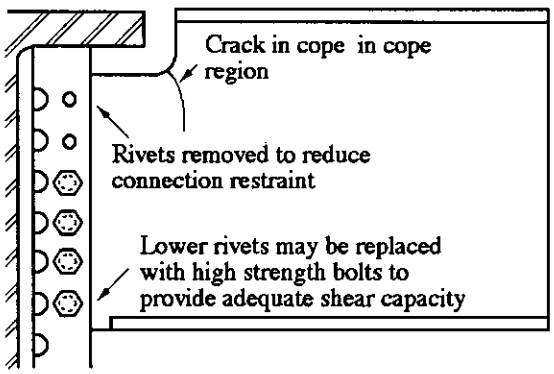

Figure 8. Bolt Removal DLM

Theories of crack initiation and crack growth are also relevant to this study. The nominal stresses in the members are always less than the yield stress while cracking occurs. As a result, elastic crack growth models are applicable to this coped connection even though limited local yielding may occur at the crack tip as a result of the large stress concentration. Crack growth generally follows three stages of behavior, as shown in Figure 9. In Stage I, the crack growth rate is very slow because the crack is initiating. This first stage requires a long period for a specimen with no initial flaws, but for many practical fatigue details, this stage can be a short period because large initial flaws effectively short circuit this first stage behavior.

In Stage II, the crack has already initiated and theoretically lengthens by the elastic crack growth model

$$\frac{da}{dN} = C\,\Delta K^n \qquad \text{(Eq. 3)}$$

where a is the length of the crack, as depicted in Figure 10, C and n are empirical coefficients that depend upon the details of the loading and the specimen, and K is the stress intensity factor

$$K = F\,\sigma\sqrt{\pi\,a} \qquad \text{(Eq. 4)}$$

The factor F depends upon the geometry of the specimen, and σ is the magnitude of tensile stress level at the crack. The coefficients, C and n, are normally determined from an empirical fit to the experimental crack growth data, as depicted in Figure 9.

The third stage of elastic crack growth is unstable crack growth during which the crack very rapidly grows to great lengths. For elastic behavior, this unstable crack growth occurs when the stress intensity factor, K, becomes larger than a critical stress intensity factor, K_{IC}, which is empirically determined from the Charpy V-Notch (CVN) toughness of the material and the loading and geometry of the specimen. This last stage of behavior may lead to dramatic failure of members and connections. As a result, this last stage of behavior is not of great importance to this study, since fatigue cracking must be stopped or controlled long before Stage III behavior has been reached.

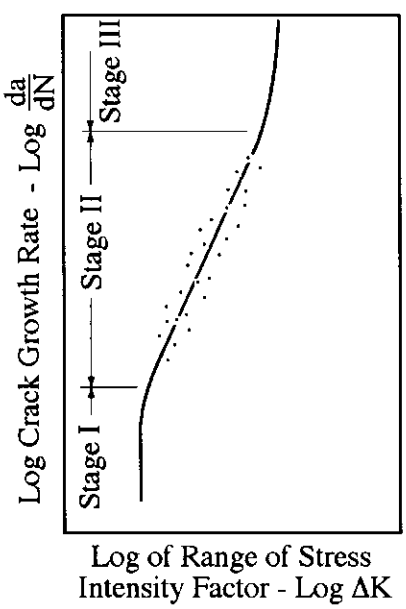

Figure 9. Typical Crack Growth Rates

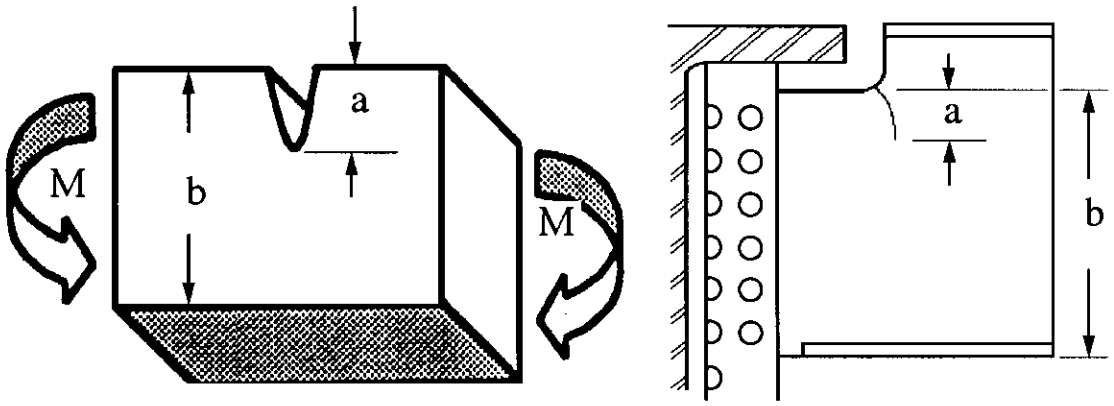

a) Idealized Crack Dimensions b) Actual Crack Dimensions

Figure 10. Typical Crack Geometry

SCOPE OF THIS REPORT

This report summarizes a comprehensive research study of the fatigue behavior of coped stringer-to-floorbeam connections and the DLMs used to limit crack growth. The report is brief but comprehensive. The next chapter summarizes the experimental methods and setup. The third chapter discusses the individual tests completed during this research, and the fourth chapter provides a more detailed analysis and evaluation of the research results. This analysis compares the effectiveness of alternative methods, and it establishes a basis for the further development of practical design and evaluation methods described in the fifth chapter. Finally, the last chapter provides a summary of the research results, the recommendations from the research, and a review of issues that are still unresolved after completion of this work.

EXPERIMENTS AND EXPERIMENTAL SETUP

GENERAL

An experimental study was performed in the Department of Civil Engineering Structural Research Laboratory at the University of Washington. The tests simulated the stringer-to-floorbeam connection, and they evaluated the fatigue cracking and effect of various DLMs on further crack growth. In these experiments, fatigue cracks were first developed in uncracked stringer copes, and then a DLM was applied and further cyclic testing was completed to determine whether and when further cracking developed.

TEST SPECIMENS

Previous research [Roeder et al 1998] showed that fatigue cracking of the coped stringer-to-floorbeam connection is caused by the negative bending moment induced by the rotational restraint in the connection. This bending moment causes tensile stress at the top of the beam at the cope. This tensile stress, combined with the roughness of the cope and the reduced section modulus of the coped region, causes fatigue cracking. Since the rotational restraint of the connection is the key contributor to fatigue crack development, an experimental program to evaluate this fatigue cracking must place considerable emphasis on the rotational stiffness of the connection.

The Lewis River Bridge was the prototype bridge for this fatigue study. The stringers of this bridge [Wong 1997] were WF24x74 sections with a span length of 8.04 m (26'-4$\frac{3}{8}$") between the centerlines of rivets at each end. The measured rotational spring stiffness of the prototype stringer-to-floorbeam connection was represented by the dimensionless ratio, $K_sL/E\,I$, and $K_sL/E\,I$ ranged from 1.56 to 2.35. The corresponding rotational spring stiffness for a 90 percent scale model should fall in the range of 44,000 to 66,000 kN-m/rad.

With fatigue testing, it is best to test full-sized specimens. However, it was also necessary to test the specimens in a way that properly simulated the connection stiffness. Therefore, initial planning recognized the possibility of testing a two-span stringer assembly such as depicted in Figure 11a, since this assembly permitted modeling of the deck slab and better simulated the continuity and rotational restraint of the connection. The two-span specimen required much more laboratory space and was more costly to build. A pure cantilever specimen, such as illustrated in Figure 11c, could also be used, because it could provide very accurate control of the stress state in the cope region. Although the cantilever specimen should have been very economical, this test configuration was rejected because the stress and deformations outside the cope region and the connection rotations would be dramatically different from those expected for the prototype bridge stringers. The single span specimen shown in Figure 11b was the preferred test configuration because it would permit a larger number of tests with the available funding. Therefore, a single-span test specimen was used as the primary test specimen, but it was approximately 90 percent scale because this scale would permit testing of the two-span specimen if that specimen was found to be necessary during the study.

The specimens were made with W21x62 sections in the general configuration shown in Figure 11b, and the span length was 7.0 m (23 ft). The individual test specimens were purchased as 7.6-m (25-ft) long sections, and up to three tests were completed with each specimen. Two specimens were obtained by turning the specimen end-for-end and making a connection from each of the beams. The third test was achieved for some specimens by cutting approximately 300 mm (1 ft.) from the one end of the specimen and fabricating another connection at this cut end.

One end of the test specimen was connected to the reaction wall, and a pin connection was used at the far end of the beam, as depicted in figures 11b and 12. This configuration was analyzed in some detail to

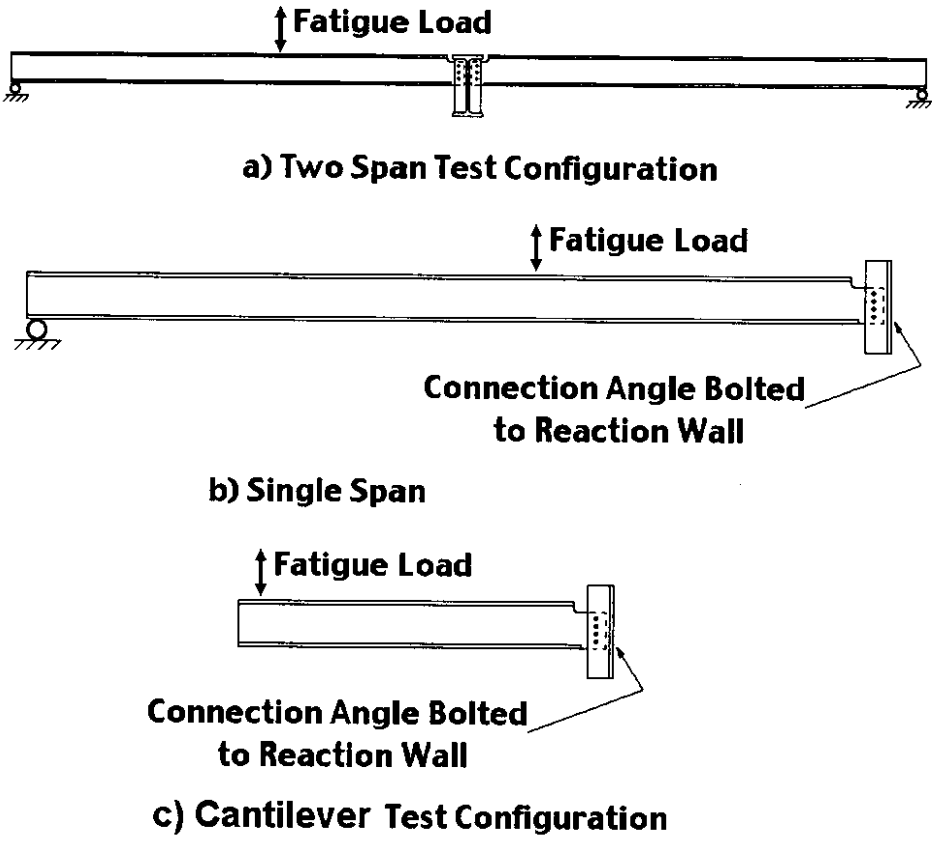

Figure 11. Schematic of Possible Fatigue Test Arrangements

- determine the response of the beam and the stringer-to-wall connection
- evaluate the stress at the critical cope region
- and develop relationships between the load and the end rotation as a function of the connection rotational stiffness, k_s, for interpretation of the test results.

The actual load on a bridge stringer is a moving load, and the minimum and maximum stresses in the stress range occur when the load is at different positions on the stringer. However, the analyses showed that a comparable maximum stress range of the cope is developed when a cyclic load is applied at a fixed point that is approximately 40 percent of the span length from the stringer connection. Application of the cyclic load at this point permitted development of stress ranges at the critical location with load applications [Wong 1997] that were comparable to those expected on the Lewis River Bridge. The actual load

point was 47.7 percent of the span length from the stringer connection because of the locations of tie downs in the strong floor, as shown in Figure 12. The pin end of the connection rested on a steel bearing. The applied load always acted downward, and so no uplift force was expected on the pin connection. Nevertheless, the pin end was clamped in place by tension rods, as illustrated in Figure 12, to assure no movement of the specimen during testing. Figure 12 also shows the general configuration of the test specimen, and the load frame used to load the specimen.

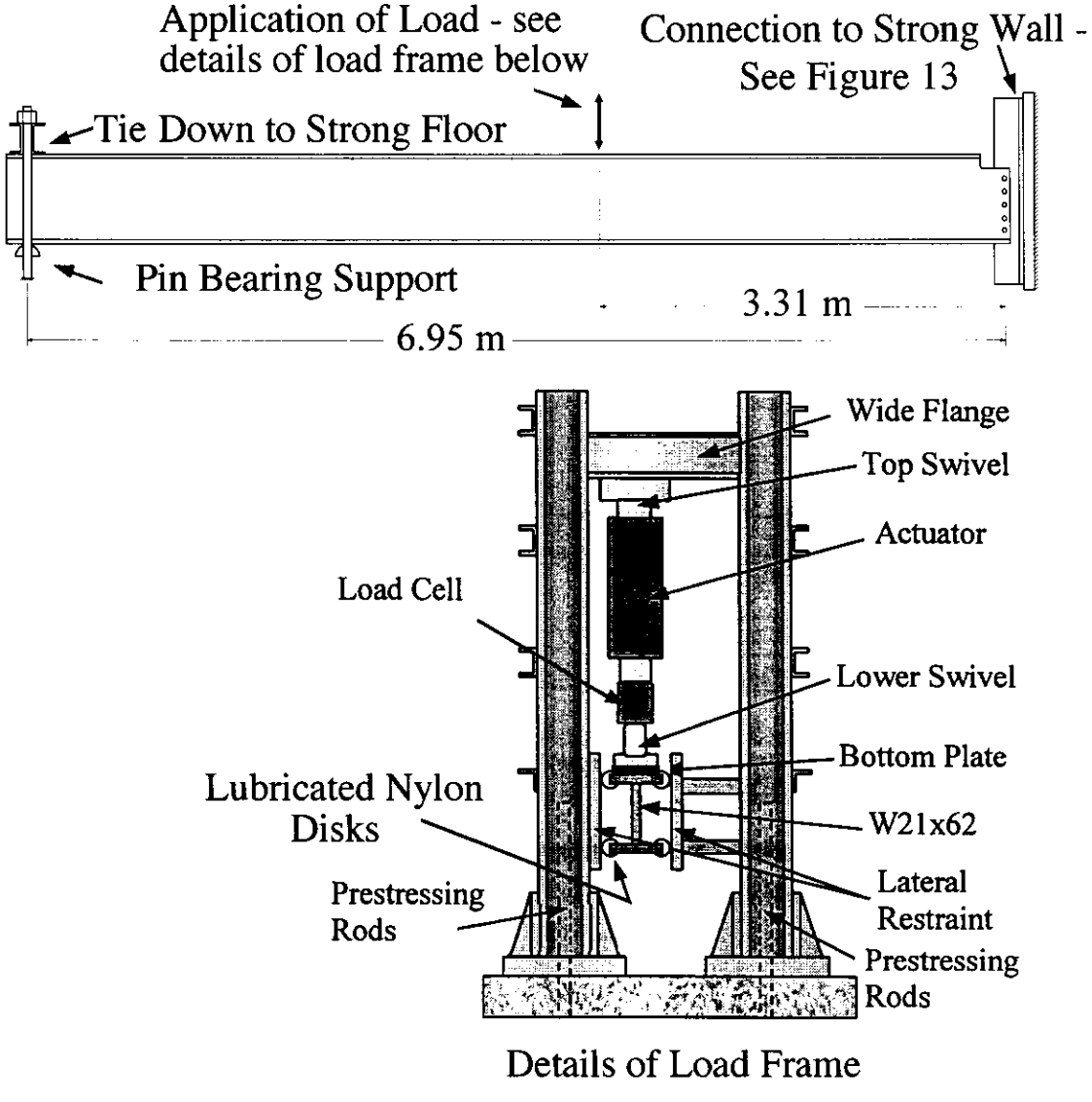

Figure 12. Test Set-Up

The stringer connection had to be designed to achieve the required k_s for the connection. The test specimen was bolted to the reinforced concrete reaction wall, as illustrated in figures 11b and 12, while the prototype connection was attached to the floorbeam web stiffener, as illustrated in Figure 2a. It was relatively difficult to achieve a stiffness for the specimen-to-wall connection that was comparable to that of the prototype stringer-to-floorbeam connection. A number of factors contributed to this difficulty. First, the rivets in the prototype connection were in double shear because floorbeam web stiffener angles were placed on both sides of the web of the stringer, as illustrated in Figure 2. However, the laboratory connection used only single shear, because this permitted better observation of the stringer cope region during testing. This clearly reduced the connection stiffness of the laboratory specimen.

Second, the prototype connection stiffness depended upon the deformation of the stringer-to-floorbeam connection on each side of the floorbeam, as well as twisting of the floorbeam, while the laboratory connection had a single T-section bolted to a relatively rigid wall. This increased the connection stiffness of the laboratory specimens relative to the prototype structure.

Third, the prototype connections were riveted, whereas bolts were used for the laboratory specimens. In all cases, the bolts were fit snug tight into the bolt holes (for both the T-section and the stringer web), and they were tightened to a proof load. The bolts were 22 mm ($\frac{7}{8}$ in) in diameter, since this provided a reasonable 90 percent scaling of the test specimen. The bolt spacing, clearances, edge distance, cope diameter, and all other dimensions had similar scaling for the test specimen, and the number of bolts were made the same for both the specimen and the prototype connection. In early tests, A307 bolts were used, since these closely matched the proof load and the general behavior obtained with rivets made of mild steel. However, later tests used A325 bolts in snug tight holes and tightened to their proof loads because the A307 bolts did not have adequate fatigue resistance acting in single shear. The proof load for A325 bolts is significantly larger than

that for rivets or A307 bolts, and so the increased friction resulting from the larger proof load increased the slip resistance to something closer to that obtained with rivets acting in double shear.

Fourth, deformation of the thick end plate and tensile elongation of the bolts connecting the stringer connection to the reaction wall contributed rotation (and reduced stiffness) of the connection, but the magnitude of this effect was difficult to accurately predict. Finally, the riveted connections were quite old, and the effects of time, deterioration, corrosion, past local yield, and deformation were unknown.

The specimen-to-wall connection stiffness varied widely even with nominally identical connection details. This variation has been noted in other research [Roeder 2000]. However, the goal of the test program was to have an experimental rotational spring stiffness, k_s, that was equal to or slightly greater than that noted in the prototype structure, since this stiffness ultimately shortened the time for testing and development of fatigue cracks. The measured k_s of the test specimen connections did not always fall within the desired range. As a result, several modifications were made to the laboratory stringer connection to change the measured stiffness, as illustrated in Figure 13. These modifications included using bushing inserts in the T-stem, sand blasting the T-stem surface for added friction, and using a larger T-section.

The load was applied by a 245-kN (55-kip) MTS hydraulic actuator through a load frame, as illustrated in Figure 12. The relatively rigid load frame was clamped to the strong floor through tensioned rods, as shown in the figure. The load frame also applied lateral support to the stringer at the load point. Lubricated nylon discs were used to assure that lateral movement and twisting of the stringer was prevented but that no significant friction or resistance developed at the lateral support location.

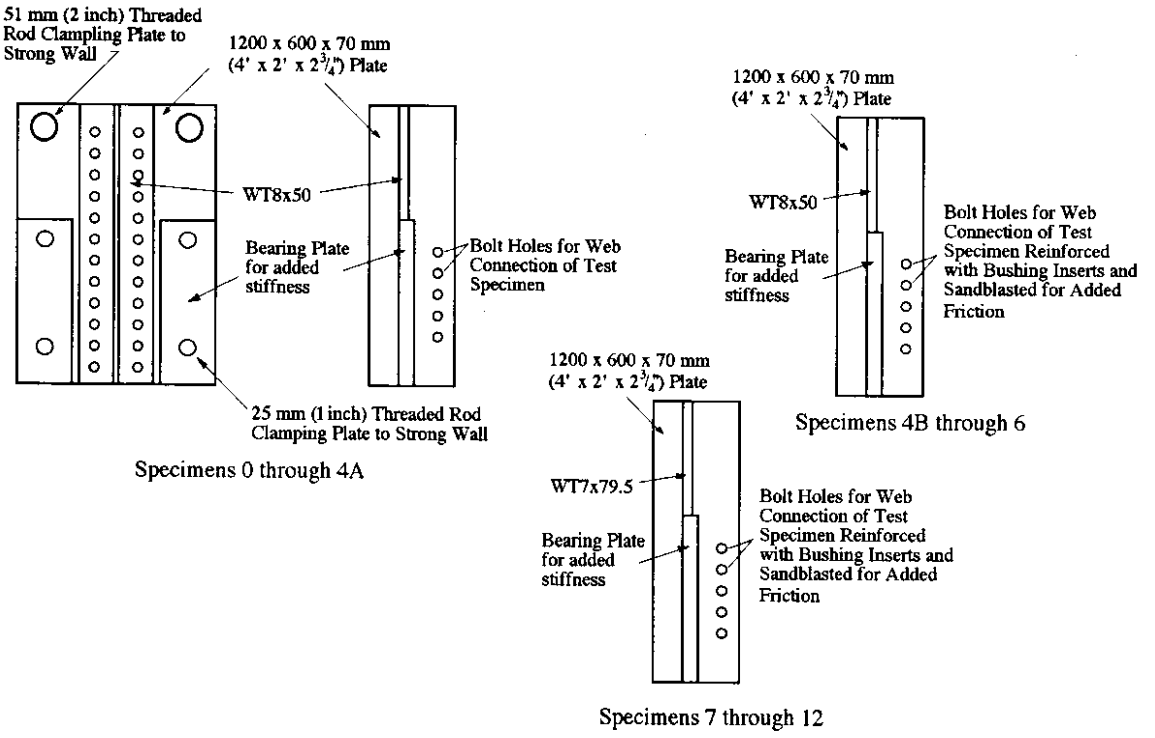

Figure 13. Details of Stringer to Wall Connection for Test Specimens

INSTRUMENTATION AND DATA

The specimens were extensively instrumented to permit accurate determination of specimen behavior during the testing. Strain gages were attached in pairs at three locations on the beam, as illustrated in Figure 14. The top and bottom gages are identified with the "SGT" and "SGB" notation, respectively, and the gage pairs permitted determination of the curvature of the beam when the gages were wired as a half-bridge configuration at these three locations. Four additional strain gages (SGC1 through SGC4) were installed to measure local strains near the cope. All strain gages were FLA-5.120-11 gages from Texas Measurements.

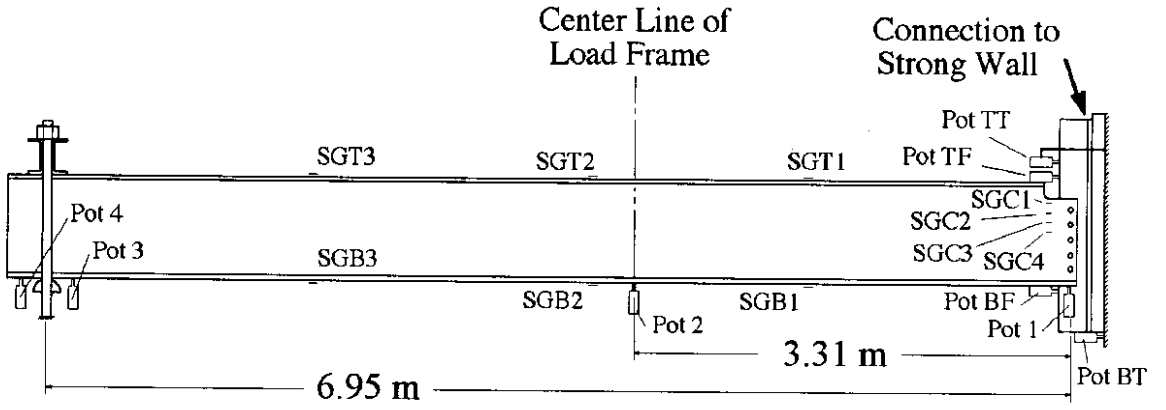

Figure 14. Instrumentation on the Test Specimens

Potentiometers were used to measure deflections, deformations, and rotations and are identified as "Pot" in Figure 14. Vertical deflections or movements were measured with Pot 1 through Pot 4. Pot 1 measured vertical movement at the web connection. Pot 2 measured the vertical deflection under the load point of the specimen, and this provided a redundant check of the vertical movement provided by the LVDT in the actuator. Pot 3 and Pot 4 combined to measure any vertical movement and rotation at the pin end of the specimen. PotTF, PotBF, PotTT, and PotBT measured movements needed to determine the end rotation of the stringer-to-wall connection. There are several sources of this rotation and connection deformation, and they are closely related to k_s. These four potentiometers allowed separation of the components of the connection rotation. Pot TF and Pot BF provided measurements of the relative rotation between the end of the beam flange and the T-section. This component of the rotation considered deformation of the bolts (or rivets) and elongation and deformation of bolt holes. Pots TT and BT measured the relative rotation between the T-section and the strong wall. This component of rotation included deformation of the T-section, deformation of the heavy end plate, and elongation or deformation of the threaded rod connecting the plate to the strong wall. The sum of these two rotation components was the rotation of the connection, and the ability to separate

these two rotation components allowed better monitoring and control of the connection stiffness. If the rotation increased during testing, it was possible to separate the source of the increased rotation and decreased stiffness. The potentiometers were 9605 Duncan Electronics devices with 13-mm (1/2-inch) total displacement capacity.

The MTS actuators were powered by hydraulic pumps, and they were controlled with an MTS Model 406.11 electronic controller. Fatigue load patterns were generated with an MTS Model 410.31 function generator. The loads were displacement controlled, and displacements were applied in a sinusoidal pattern, with most loading at the rate of 2 Hz. The magnitude of the load (and the corresponding displacement) varied from test to test, and sometimes it was varied within the test. The MTS actuators had an internal load cell for measuring applied load and an internal LVDT for measuring actuator displacement. The MTS load cell and the internal LVDT were calibrated before testing, and the calibration was checked at critical intervals during testing. All calibration was completed on test equipment that was certified to standards traceable to the US National Bureau of Standards just before testing started. The calibration of potentiometers used to measure deflections and rotations was checked before the start of each test and at intervals during each test.

All data was recorded on a 200-MHz Pentium computer in the Windows 95 operating system with LabView (version 5.01) software. A PCI LabView board was installed into the computer and was connected to a National Instruments (NI) 1001 Chassis. Potentiometers, the load cell, and all actuator data were measured through a NI1300 terminal block. Power was supplied to the potentiometers with a 10-volt DC power supply. The data acquisition system continually monitored all data during testing. However, during most cycles only maximum and minimum values were noted to determine any variation in the behavior of the specimen. After completion of each 25,000 cycles, five complete cycles of data were measured and recorded for further detailed analysis of test results. These measurements were later compared for evaluation of changes in loading,

connection stiffness, and specimen behavior as the test progressed. Additional cycles of data were recorded when any change was suspected.

The specimens were visually observed at regular intervals to determine whether cracking had visibly initiated. The intervals between inspections were shorter after cracking occurred or during periods when changes were expected. The researchers maintained a daily log that summarized these daily observations. These visual inspections focused on initiation of cracking and increases in the length of existing cracks. Dye penetrant was used to help determine whether cracking had initiated and to establish the length of the crack.

INTERPRETATION OF DATA

The measurements were translated into data that were meaningful in interpreting the test results. The strains provided by the flexural gage pairs were translated into bending moments and moment diagrams. These strain gage pairs were measured through a half bridge configuration in which the resulting measurement was the difference between the strain at the top and the bottom of the beam, $\Delta\varepsilon$. The loads were always smaller than the yield load, and so the measured strains could be directly translated into curvature, ϕ, by

$$\phi = \frac{\Delta\varepsilon}{d_b} \qquad \text{(Eq. 5)}$$

where d_b was the depth of the steel beam. The curvature could be readily translated into bending moment with the elastic modulus of the steel and the moment of inertia of the wide flange. That is,

$$M = \phi\, EI \qquad \text{(Eq. 6)}$$

These moments could be combined with the measured applied load to determine the moment diagram for the specimen under the applied loading. The resulting moment

diagram provided the bending moments at the specimen-to-wall connection, the pin support, and the cope region.

Rotations were determined by dividing the difference in deflection provided by the top and bottom potentiometers by the distance between the instruments. That is, both components of stringer-to-wall connection rotation, θ_i, were

$$\theta_i = \frac{\Delta_{top} - \Delta_{bottom}}{d_g} \qquad \text{(Eq. 7)}$$

where Δ_{top} and Δ_{bottom} were the measurements from the top and bottom potentiometers and d_g was the vertical distance between the center of the potentiometers for the respective potentiometer pair. Equation 7 assumes small angle rotation, but this is a valid assumption, since the error made with this assumption is significantly less than the 0.01 percent for maximum rotations measured in this study. The total rotation was determined by summing the two components of rotation.

The total specimen-to-wall rotation, θ, provided a second method of determining k_s, and the moment caused by this connection end restraint. To develop this capability a series of analyses of the partially restrained beam shown in Figure 15 was performed. The analyses were linear elastic analyses of a one-degree statically indeterminate system. The analyses were completed by closed form solution and were verified by a finite element analysis. For the beam size, span length, and load placement used in these tests, the parameter analysis provided an equation for k_s as a function of the measured connection rotation, θ. This relationship is

$$k_s = \frac{P}{\theta} \left\{ \frac{L_p}{2} - \frac{L_p^3}{L^2} \right\} - \frac{3 E I}{L} \qquad \text{(Eq. 8)}$$

where the dimensions are defined in Figure 15. The spring stiffness depends upon the $\frac{P}{\theta}$ ratio, and if this connection becomes small enough, a negative stiffness is predicted. Under these conditions a zero stiffness should be employed. The reason for this observation is that beams with very small spring stiffness have no effect on the beam deformations or moment diagram, and the beam behaves as a pin ended member. By the same token, an extremely large spring stiffness also results in no changes in the beam deflection and moment diagram, because the stiffness is adequate to effectively produce a fixed end connection. Intermediate spring stiffnesses have a great impact on the connection deflection and moment diagram, and the coped stringer connections fall into the lower portion of this intermediate range.

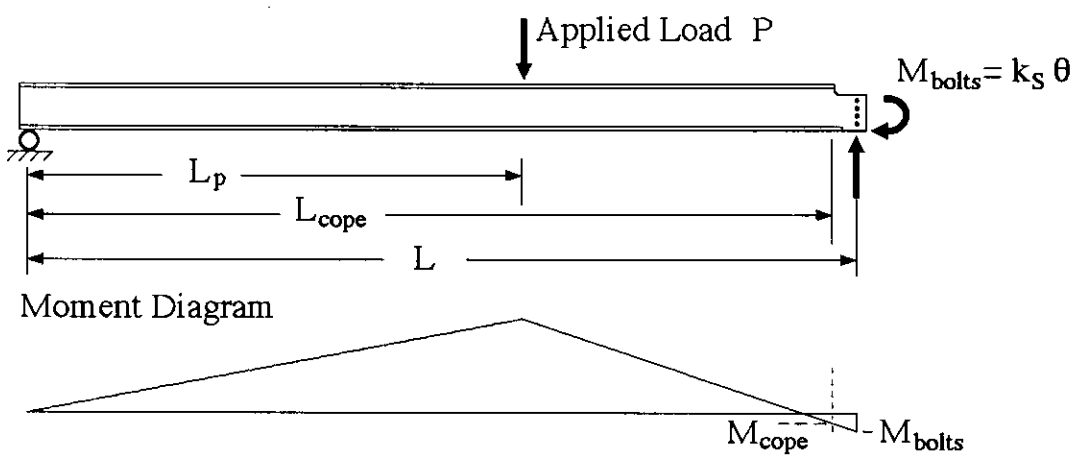

Figure 15. Geometry and Moment Diagram for Test Specimen

The measured connection rotation can be inserted into Equation 8 to determine k_s, and the moment at the bolt group, M_{bolt}, can then be directly determined by multiplying the rotation and the spring stiffness as shown in the figure. The moment at the cope area, M_{cope}, can then be determined by equilibrium so that

$$M_{cope} = P\,L_p \left\{ 1 - \frac{L_{cope}}{L} \right\} - \frac{k_s\,\theta\,L_{cope}}{L} \qquad \text{(Eq. 9)}$$

For evaluation of fatigue cracking, this moment is computed at the location, L_{cope}, where the tip of the crack is the location of interest for defining the dimension. The nominal stress and stress range are computed by dividing this moment by the section modulus of the reduced section in the coped region. A negative moment produces a tensile stress at the top of the beam in the region of the cope, and this nominal stress is the stress resulting in fatigue cracking of the coped stringer connection.

As discussed, two methods were available for translating the measured data into moment and stress at the cope region. Both methods were used, compared, and evaluated. The measured rotation method was determined [Skare 1999, Kalagoris 2000] to be the more consistent and reliable method and is the method described throughout this report.

THE TEST PROGRAM

This chapter has summarized the test setup, instrumentation, and data analysis used in this research study. In general, each specimen was tested to develop a fatigue crack in the region of the cope, and then the specimen was modified with one of several DLMs. The testing then was continued to evaluate the effectiveness of the DLM. Many individual variations in testing were required to achieve the goals of the research program and to respond to the research results. As a result, a more detailed description of the individual tests is provided in the next chapter.

INDIVIDUAL TESTS

TEST SPECIMEN DETAILS

W21x62 sections [AISC 1995] of A572 Grade 50 steel and 7.6m (25 ft) long were used for the test specimens. The cope was 85.7 mm deep and 133.4 mm long. The distance from the bolt centerline to the end of the beam was 57.2 mm. The spacing between the five bolts ranged between 69 mm and 76 mm, as shown in Figure 16a.

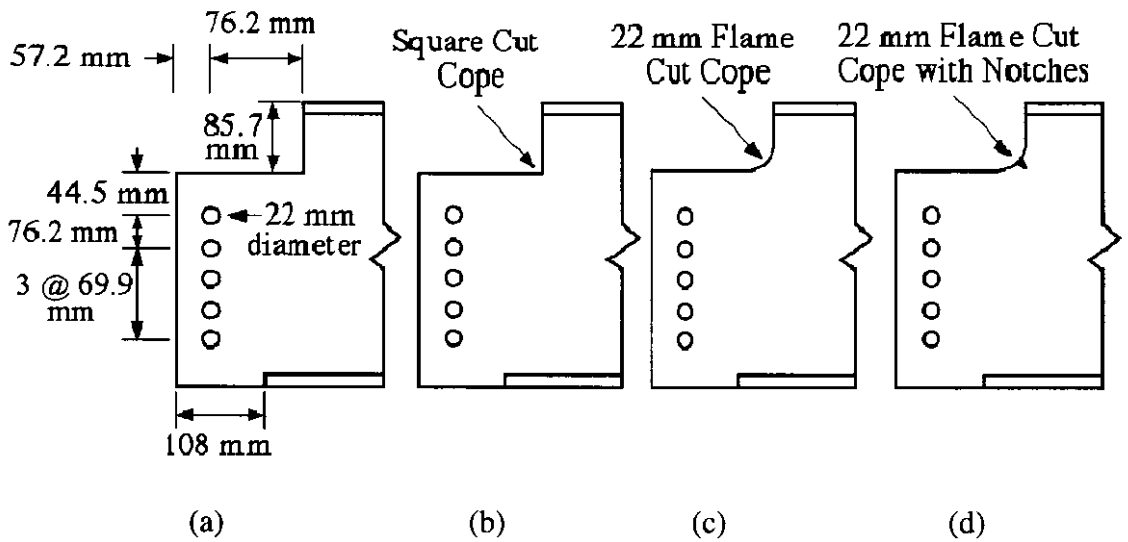

Figure 16. Schematics of Cope Detail

The test specimen material was not the same as that of the stringers used on the Lewis River Bridge because of the age of the prototype structure and the changes in steel that evolved during that period. Fortunately, fatigue performance of structures is not strongly dependent on the material yield strength, and fatigue cracks are not normally permitted to grow to a length at which CVN toughness becomes critical. Therefore, modern steels can be used for simulation of these older steel connections without adversely affecting the validity of the test results. Mill certificates indicated that the

specimens had yield stress of 379 MPa (54.9 ksi) and tensile strength of 517MPa (74.9 ksi). Material tests were carried out on samples cut from each steel section. The tests were conducted according to ASTM standard A370, and these tension tests gave an average yield strength of 402MPa (58.2 ksi), average ultimate strength of 541MPa (78.4 ksi), and an average ultimate strain in the direction of rolling of 28.6 percent. Charpy V-notch tests also met the ASTM E23 requirements.

The test specimens were designed to establish the conditions under which cracking could be expected, to determine the effectiveness of various DLMs, and to establish predictive models for the remaining fatigue life of the riveted, coped stringer connections before and after cracking. Different cope details were used in different specimens, as shown in Figure 16 and listed in Table 1. The first two tests performed in this study used square cut copes, and the remaining 14 used 22-mm radius flame cut copes. The tests normally developed fatigue cracking so that a DLM could be applied to the specimen. The rate of crack initiation and growth depends upon the stress level, the number of cycles, and the geometry of the cope. The first two square cut specimens permitted more rapid crack development, and these two tests provided a baseline for the rate of initial crack development. The remaining specimens had a radius cut cope. The radius cope had a geometry similar to that of the prototype connections. However, the finish of the flame cut radius was much smoother than that noted on actual bridge stringers. The rate of crack development was more rapid with rough cope cuts, and therefore, Table 1 includes the measured finish of the cope. The cope roughness was measured using GAR electroforming microfinish comparators. Lower numbers correspond to smoother surfaces. ST stands for shape-turn, which indicates how the cut or surface was made. Because of the relatively smooth flame cut finish of some specimens, some specimens did not crack, cracked at locations unsuitable for a DLM, or took an inordinately long time to crack. As a result, the last eight specimens (specimens 4 through 12) were notched in different ways in the coped region to speed up crack

Table 1. Cope Details of Test Specimens

Test No.	Cope Geometry	Disposition of Specimen	Roughness of Cope Finish
0A	Square Cut Cope	Tested to failure	250 ST
0B	Square Cut Cope	Tested to failure	250 ST
1	22 mm Flame Cut Cope	Tested to failure	250 ST
2	22 mm Flame Cut Cope	Cracked. Drilled hole below crack tip. Cracked out of hole. Drilled 2nd hole below new crack tip & cracked again.	250 ST
3	22 mm Flame Cut Cope	Cracked in difficult location . No DLM testing completed	250 ST
3B	22 mm Flame Cut Cope	Cracked. Drilled hole below crack tip from NCHRP equation &cracked again.	250 ST
4	22 mm Flame Cut Cope	No crack after 3,353,000 cycles.	250 to 500 ST
4B	22 mm Flame Cut Cope	Cracked. Removed top 2 bolts, and crack lengthened only slightly.	250 to 500 ST
5	22 mm Flame Cut Cope w/ 3-1.6mm notches @ 45°, 61°, & 70° from horizontal	Cracked. Removed 1st top bolt Crack lengthened significantly. Removed 2nd bolt, crack lengthened slightly.	125 ST
6	22 mm Flame Cut Cope w/ 3 – 2mm notches @ 32° & 62° from horizontal	Cracked. Drilled hole below crack tip, inserted & proof-loaded bolt. Cracks Develop in LI Washers. Replace bolt and washer & no further cracking of beam.	250 to 500 ST
7	22 mm Flame Cut Cope w/ 2-2.5mm notches @ 30° & 45° from horizontal	Cracked. Drilled hole below crack tip, inserted & proof-loaded bolt, Developed crack	125 ST
8	22 mm Flame Cut Cope w/ 2-2.5mm notches @ 30° & 45° from horizontal	Cracked. Removed 1st top bolt and crack lengthened. Removed 2nd bolt, and crack lengthened significantly after 2 million additional cycles.	250 ST
9	22 mm Flame Cut Cope w/ 2-2.5mm notches @ 30° & 45° from horizontal	Cracked. Drilled hole below crack tip, inserted and proof-loaded bolt. Developed crack out of bolt hole.	250 to 500 ST
10	22 mm Flame Cut Cope w/ 2-2.5mm notches @ 30° & 45° from horizontal	Cracked. Removed 1st top bolt, and crack lengthened significantly.	250 ST
11	22 mm Flame Cut Cope w/ 2-2.5mm notches @ 30° & 45° from horizontal	Cracked. Removed top 2 bolts, Developed new crack near bolt holes.	250 ST
12	22 mm Flame Cut Cope w/ 2-2.5mm notches @ 30° & 45° from horizontal	Cracked. Removed top 3 bolts. No crack growth.	500+ ST

initiation and encourage the crack to develop in a convenient place for applying a DLM. In the last seven tests (specimens 6 through 12), a steel cutting blade was run across the tip of the notch three times to further sharpen the tip of the notch. The roughness values reflect the surface of the cope but ignore effects of the notches.

The three DLMs tested were the drilled hole method, the drilled hole with inserted bolt method, and the bolt removal method, and the specimens are correlated to their respective DLM methods in Table 1. The test sequence noted in this table is slightly different from the initial planned schedule, since the direction in which cracking initially occurred affected the DLMs that could be applied for a given specimen.

The first three tests, Specimens 0A, 0B and 1, were conducted to failure. These gave benchmarks for crack initiation and crack growth with no DLM, and these tests also allowed observation of the failure mode.

Specimens 2 and 3 were tested to determine the effectiveness of the drilled hole DLM. For Specimen 2, the diameter of the hole used in the WSDOT procedure (24 mm (15/16 in)) was tested. Since the specimens were at 90 percent scale, the bolt hole diameter used in the model was 21 mm. The test on specimen 3 was carried out to determine the effectiveness of a larger hole. In this case the required hole radius, ρ, was based on a recommendation from an earlier research study [Fisher et al. 1980]. This equation was based on a somewhat different stress state, but it suggested that no further crack propagation would occur if the hole radius, ρ, exceeded the value given in Equation 10.

$$\rho \geq 191 \times 10^{-6} (\Delta K)^2 / \sigma_y \text{ (MPa, m)} \qquad \text{(Eq. 10)}$$

The stress intensity factor, ΔK, is chosen from the appropriate loading case, and

$$\Delta K = F\,\Delta\sigma\sqrt{\pi a}$$

$$\Delta K = \left[\frac{0.923 + 0.199\,(1 - \sin\frac{\pi a}{2b})^4}{\cos\frac{\pi a}{2b}}\right]\sqrt{\frac{2b}{\pi a}\tan\frac{\pi a}{2b}}\;\Delta\sigma\sqrt{\pi a} \qquad \text{(Eq. 11)}$$

where a is taken as the distance from the top of the cope to the far side of the hole, as shown in Figure 17 [Fisher et al 1970], and b is the depth of the coped section for the coped connection under consideration. As a increases, the required hole diameter increases.

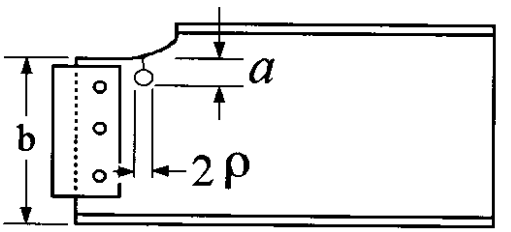

Figure 17. Dimensions for Computing Required Hole Diameter, 2ρ

For the W21x62 section, a hole of 31.8 mm diameter was initially computed to be necessary if a was 36.6 mm for the load that was applied to the section for Specimen 2. However, after the test the researchers recognized that the moment range, ΔM, had been computed at the incorrect location. It should have been computed above the crack to give a hole diameter of 40.4 mm (1.6 in). In Test 3A, the crack occurred in an inconvenient location for the drilled hole DLM. Test 3B was therefore used to test this DLM.

In both cases that the drilled hole method was used, liquid dye penetrant and visual inspection were used to find the crack tip. The center of the hole was placed slightly below the visible crack tip when possible. This gave greater confidence that the actual crack tip would be included in the drilled material. Holes were polished with an

abrasive sanding band. After cracking had initiated at the far side of the hole, it was sometimes possible to drill another hole and again evaluate the effectiveness of the drilled hole method.

Specimens 4, 5, 8, 10, 11 and 12 were tested to evaluate the effectiveness of the bolt removal DLM. This method attempts to reduce the stiffness of the end connection by reducing a number of bolts from the top of the beam. This reduces the rotational stiffness of the connection, as well as the moment and tensile stress in the cope region. Specimen 4A did not crack, so Specimen 4B was used for the testing of this DLM.

Specimens 6, 7, and 9 were tested to evaluate the effectiveness of the drilled hole with proof loaded bolt DLM. After the crack had reached a predetermined length, a 21-mm diameter hole was drilled, and a 51-mm (2-in) long, 19-mm (3/4-in) diameter ASTM A325 high strength bolt with was placed in the hole. Then the bolt was snug tightened with a hand wrench and pretensioned to ensure that the bolt was taken to at least 70 percent of its ultimate strength. Load indicating (LI) washers were calibrated, and the gap between the head of the bolt and flat portion of the load indicating washer was used to indicate that the bolts had reached their proof load. Flat hardened washers also were used behind the load indicating washers, as well as between the nut and the web of the beam.

Table 1 also summarizes the general disposition and history of individual test specimens. More detailed information on individual test history is provided in the next chapter. The DLM and sequence of DLM applications for individual specimens is provided in the table. As noted from the table, new cracks developed or lengthened after some DLMs were employed for some test specimens. In Table 1, cracks noted as lengthening slightly were connections where the crack lengthened 10 percent or less over a large number of load cycles. Cracks are noted to have lengthened significantly when the crack lengthened by more than 50 percent over a series of load cycles.

SPECIMEN LOADING

After specimens had been placed in the rig shown in Figure 12, a preload of 133 kN (30 kips) was applied and then removed. This preload was chosen because it causes cope stresses significantly greater than the constant amplitude fatigue limit level regardless of the fatigue category used for the specimen. This is important because Equation 2 includes all stress cycles, and the present thinking regarding variable amplitude fatigue is that stress cycles smaller than the constant amplitude fatigue limit do not contribute to fatigue cracking unless at least one load cycle that was larger than this fatigue limit had been previously applied. With this preload, all of the smaller magnitude load cycles applied later were therefore expected to contribute to the crack development.

The actuator operated under displacement control and imposed displacements in a 2 Hz sinusoidal pattern on the beam, as shown in Figure 18. Every time the loading was restarted, the displacement magnitude was gradually increased to the desired level. This reduced the possibility of very large force spikes when the testing got under way. The frequency of 2 Hz created an average test duration of three to five weeks.

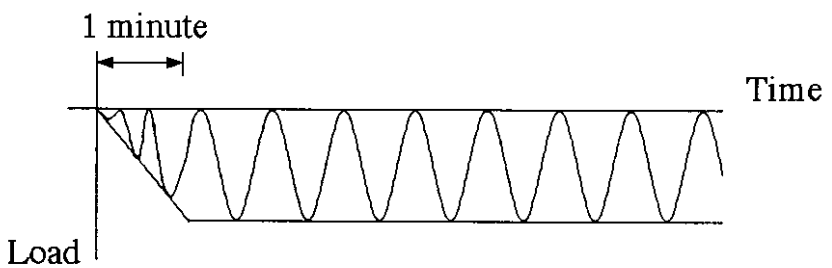

Figure 18. Ramped Sinusoidal Loading

The initial tests (specimens OA through 1) [Skare 1999] used variable amplitude loading. During testing of specimens 2 through 12, a load was chosen for the test on the basis of the results of the previous tests, and the beam was loaded at this level for one to two million cycles. If no crack had initiated by that time, the load was increased to hasten

cracking. The load was normally increased in 9-kN (2-kips) increments, and the larger loads were applied if cracking was not noted after 500,000 to 1 million additional cycles. The applied loads were increased more frequently after the specimen had been loaded for a total of 2.5 million cycles. Increased loading was also applied to several specimens to more strenuously test various DLMs. In all cases, Equation 2 was used to compute an effective stress to evaluate the full fatigue load history.

SUMMARY DESCRIPTION OF TEST RESULTS

The behavior of each test unit is thoroughly described elsewhere [Skare 1999 and Kalogiros 2000], and this information is summarized in Table 2. Here the rotational stiffness, k_s, was found by using Equation 8. The nominal stress is provided in the table, and this nominal stress is the stress at the position on the cope where cracking initiated at the number of cycles considered. This stress was computed by knowing the applied force and the stiffness, k_s. Negative stress values imply compression at the top of the beam. The effective stress is determined from the nominal stress values determined over a period of testing with Equation 2.

Specimens 0A and 0B had a square cope. They were tested to determine how long cracks took to initiate and grow in order to plan the remaining tests, as well as to ensure that loading procedures and data collection procedures were adequate. The data obtained from these tests were useful only as global indicators of connection performance, since the geometry was an extreme limit to the prototype connections, and the specimens were designed to verify the functionality of the test system. Initial cracking in Specimen 0A was observed at the cope after 11,000 cycles at 89 kN (20 kips). Testing was continued, and the crack grew as shown in Figure 19 and Table 2.

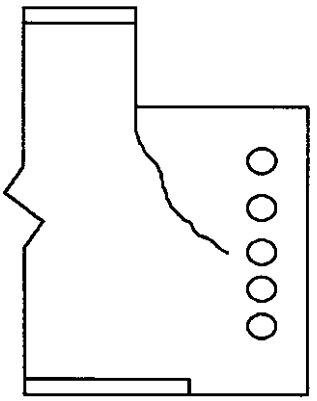

Figure 19. Specimen 0A Cracking

Specimen 0B loading started at 33 kN (7.4 kip) and was systematically increased to 122 kN (27.4 kip). Plastic deformation at the cope corner was seen at 243,000 cycles. The crack shape was similar to that for Specimen 0A. The crack grew to a length of 249 mm (10 in) by cycle 1,547,000, as shown in Table 2.

Specimen 1 had a 22-mm (7/8-in) radius flame cut cope, and A307 bolts attached the beam to the tee section. Loading started at 60 kN (13.5 kip) and was systematically increased to 150 kN (33.7 kip). After 914,000 cycles slip was noted at the bottom bolt. When it was tightened at 916,000 cycles it fractured at the first thread from the head. The bolts were replaced, but after only 3000 additional cycles cracks were found in the top and bottom bolts. The A307 bolts were replaced with A325 bolts, and a crack initiated at the cope after 1,675,000 cycles. The crack grew from the base of the cope into the third bolt hole by cycle 1,856,000, as shown in Table 2. All future specimens beyond Specimen 1 used A325 bolts, which were tensioned to their proof load and fit in snug tight holes, for the web connection to provide better friction and fatigue resistance under single shear bolt behavior.

Specimen 2 had a 22-mm radius (7/8-in) flame cut cope, and A325 bolts attached the beam to the tee section. Loading was carried out at 124 kN (27.9 kip), and cracking initiated at 450,000 cycles. The crack grew vertically at the base of the cope radius. At

516,000 cycles, the crack length was 32 mm (1.25 in), and a 22-mm (7/8-in) diameter hole was drilled with a centerline 3 mm (1/8 in) past the visible crack tip. The hole was smoothed and polished. After 58,700 cycles, a new crack initiated in the same direction as the first crack at the bottom of the drilled hole. At 587,000 cycles it was 4.8 mm (0.2 in) long, and a second 2-mm (7/8-in) hole was then ground out and polished smoother than the previous hole, as shown in Figure 20. A crack at the bottom of the second hole initiated at 690,000 cycles in the same direction as the original crack, as shown in the figure. The final crack was 68 mm below the second hole at 870,000 cycles.

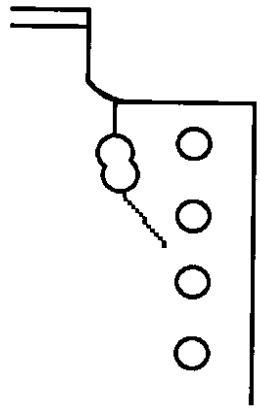

Figure 20. Specimen 2 Cracking

Specimen 3 had a 2-mm radius flame cut cope, and the cope radius was smoothed after the flame cutting. Loading was carried out at 89 kN since the previous test cracked early. At 1,430,000 cycles, Lueder's lines were observed from the cope region, indicating local yielding of the steel. The load was incrementally increased to 115 kN (25.8 kip), but after 2,508,000 cycles there was no cracking. The T-section cracked and was replaced, and loading was restarted and incremented upward. At 3,672,500 cycles, a crack initiated in the beam above the bolts. It grew down into the bolt hole at 3,777,000 cycles, as shown in Figure 21. Testing was then stopped, since the drilled hole DLM could not be applied at this area.

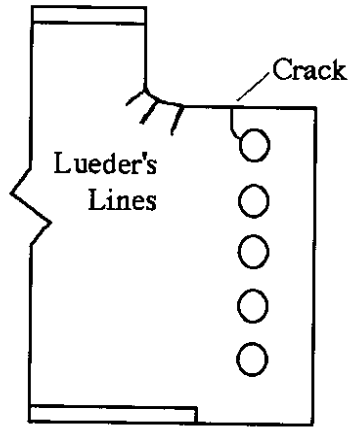

Figure 21. Specimen 3 Cracking

Specimen 3B was similar to Specimen 3. Initial loading was started at 106 kN (23.8 kip) to initiate cracking more quickly than Specimen 3, but not as quickly as for Specimen 2. After 2,020,000 cycles the load was increased to 115 kN (25.8 kip) because no crack formed, and a crack started at the base of the cope radius at 2,050,000 cycles. At 2,153,000 cycles the crack was 27 mm (1.1 in) long, and a 31.7-mm (1 1/4-in) diameter hole was drilled and polished. The hole was not centered at the crack tip to avoid a larger hole being required by the NCHRP equation. The bottom of the hole was 36.5 mm below the cope, and it was 9.5 mm below the visible crack top. A crack propagated from the bottom of the hole after 192,000 cycles after drilling. The crack was allowed to propagate to 76 mm (3 in) before testing was stopped.

Table 2. Behavior of Specimens 0A-12

(1) Test No.	(2) Test Description	(3) Load History	(4) Crack History	(5) Damage Limitation Method (DLM)	(6) Stiffness History (kN-m/rad.)	(7) Nominal Stress History (MPa)	(8) Effective Stress History (MPa)
0A	Tested to failure	89kN 385,000	Initiation	None	26,900	71.4	47.6
		492,000	25.4mm		23,700	70.9	53.5
		555,000	50.8mm		20,900	81.5	55.6
		582,000	76.2mm		18,600	69.2	56.6
		606,000	101.6mm		16,100	60.4	56.9
		632,000	127mm		12,700	49.0	56.9
		659,000	152mm		11,200	43.2	56.5
		682,000	171.5mm		9,700	38.2	56.5
0B	Tested to failure	33-122kN 980,000	Initiation	None	23,734	62.6	47.5
		1,095,000	25.4mm		23,409	69.1	50.4
		1,175,000	50.8mm		21,810	65.0	51.9
		1,218,000	76mm		20,365	70.5	52.7
		1,255,000	101.6mm		18,137	64.4	53.2
		1,290,000	127mm		15,393	55.6	53.3
		1,326,000	152mm		13,591	49.0	53.3
		1,369,000	178mm		10,764	44.8	53.1
		1,406,000	203mm		8,952	36.8	52.9
		1,455,000	229mm		7,640	30.8	52.5
		1,547,000	249mm		6,447	25.3	51.5
1	Tested to failure	60-150kN 1,675,000	Initiation	None	27,214	125.3	89.7
		1,760,000	101.6mm		21,698	103.8	91.5
		1,781,000	127mm		19,577	95.6	91.6
		1,811,000	152.4mm		16,352	83.2	91.6
		1,856,005	170mm		13,933	70.4	91.6
2	Drilled hole (WSDOT)	124kN 450,000	Initiation		27,480	106.5	108.0
		507,000	Crack = 32mm	22mm hole drilled	26,729	101.3	107.6
		575,000	Initiation 2		23,084	92.5	108.3
		587,000	Crack = +4.8mm	New 22mm hole drilled			
		690,000	Initiation 3		21,422	87.6	109.5
		745,000	+25.4mm		20,008	82.9	110.0
		817,000	+50.8mm		18,508	78.1	109.5
		870,000	+68mm		17,996	75.7	108.2
3A	Tested to failure	3,672,500	Initiation		17,795	57.8	61.9
		3,777,500	To bolthole		28,364	110.0	77.0

Table 2. Behavior of Specimens 0A-12 (continued)

3B	Drilled hole (NCHRP)	2,050,000	Initiation		24,500	85.4	86.9
		2,152,000	25.4		22,320	81.3	86.7
		2,153,000	27	31.75mm hole drilled			
		2,345,000	Initiation 2		20,434	71.2	86.9
		2,400,000	+25.4mm		18,710	65.9	86.7
		2,533,000	+50.8mm		18,230	65.5	86.3
		2,723,000	+76.2mm		17,400	62.6	85.6
4	Attempt hole and inserted bolt DLM - but no cracking	Loads up to 142kN, Total No. of Cycles 3,352,782			16,900	95.2	64.93
4B	Bolt removal DLM	Loads up to 125kN for final 2,502,300 cycles	Initial cracking at 3,102,180 cycles		19,995	85.4	76.94
		3,140,187 cycles	87mm crack	Remove top two bolts	14,789	67.2	76.91
		4,576,127 cycles	Final crack length was 91mm		5971	28.95	68.89
5	Bolt removal DLM	Load up to 125kN	Initial cracking at 1,550,000 cycles		20,762	92.97	78.69
		116kN to 1,725,000 cycles	Crack #2 initiates		19,650	87.72	79.63
		125kN to 1,924,840 cycles	Crack #1 = 57mm, Crack #2 =21mm	Remove top bolt	16,797	77.48	80.03
		133kN to 1,997,660 cycles	Crack #1= 60mm, Crack #2 =51mm	Remove 2nd bolt	12,535	64.07	21.4
		3,170,772 cycles	Crack#1 = 62mm, Crack #2 = 54mm		9,048	52.50	37.02

Table 2. Behavior of Specimens 0A-12 (continued)

6	Tested Drilled hole with inserted bolt DLM	Load to 116kN 75,000 cycles	Initial cracking		21,377	93.76	74.78
		Cycle 242,900	33mm crack	Drilled hole placed bolt	15,103	59.8	73.49
		901,700 cycles	Crack in LI Washer	Bolt/washer replaced	9,863	47.2	61.72
		1,985,000 cycles	No cracks		1,360	0.26	50.41
		2,188,401 cycles	No cracks after DLM		0	0	48.79
7	Tested Drilled hole with inserted bolt DLM	116kN always. 25,000 cycles	Initial cracking		26,533	105.3	100.74
		80,231 cycles	30mm crack	drilled hole & bolt	17,490	72.8	88.56
		561,000 cycles	Washers Crack		13,200	56.4	63.27
		1,500,000 cycles	2nd crack initiates				
		1,715,100 cycles	111mm 2nd Crack		0	-6.64	53.97
8	Tested bolt removal DLM	107kN load 5,000 cycles	Initial cracking		33,761	114.6	96.71
		75,922 cycles	22mm crack		46,642	47.4	102.25
		102,070 cycles	37mm crack	removed top bolt	44,354	41.3	97.04
		468,203 cycles	51.6mm crack	removed 2nd bolt	29,990	22.9	66.51
		1,080,000 cycles	54mm crack		0	-6.84	50.37
		2,376,480 cycles	65mm crack		0	0	38.69

Table 2. Behavior of Specimens 0A-12 (continued)

9	Tested Drilled hole with inserted bolt DLM	98kN 50,000 cycles	Initial cracking		37,932	11.2	113.96
		114,200 cycles	36mm crack	drilled hole with bolt	31,384.2	71.4	109.92
		418,000 cycles	Flat Washers Crack		25,165.8	78.5	93.16
		585,000 cycles. 107kN	Crack in LI Washer		24,195.8	76.2	89.12
		1,590,000 cycles	New crack initiates				
		1,729,710 cycles	86mm crack from bolt hole		10,404.3	41.2	75.81
10	Tested bolt removal DLM	98kN 150,000 cycles	Initial cracking		27,660	87.8	89.6
		220,000 cycles	25mm crack		24,414	78.2	86.55
		233,851 cycles	30mm crack	removed top bolt	16,039	45.9	86.04
		2,157,920 cycles	52mm crack		1,933	4.10	47
		2,333,000 cycles	69mm crack		163	-5.4	45.82
		2,651,537 cycles	Crack is 129mm		0	0	43.88
11	Tested bolt removal DLM	98kN - 107kN 50,000 cycles	Initial cracking		9,435	36.4	31.41
		92,623 cycles	13mm crack		7,202	27.4	29.76
		126,601 cycles	30mm crack	removed top two bolts	6,129	21.2	28.28
		1,955,000 cycles	Crack 1 53mm. Crack #2 initiated from 2nd bolt hole	Remove third bolt			
		2,218,430 cycles	No crack #1 growth. Crack 2 44mm		0	-3.96	9.73

Table 2. Behavior of Specimens 0A-12 (continued)

12	Tested bolt removal DLM	98kN-125kN 200,000 cycles	Initial cracking		20,615	75.1	83.2
		287,788 cycles	53mm crack	removed top three bolts	15,966	62.1	79.2
		2,694,040 cycles	No crack growth		0	-3.98	37.6

Specimen 4 sustained 3,352,782 cycles at loads systemically incremented from 111 kN to 142 kN (25 to 32 kip). No cracks were visible. The rotational stiffness was about 16,900kN-m/radian, which was lower than the stiffnesses of 22600 to 25400 kN-m/rad observed in the previous specimens that cracked earlier. Bolt holes in the T-section were 0.05mm larger than those in the beam web.

Specimen 4B was tested with a new T-section connected to the wall, and rods passing through the strong wall were tightened to increase the end rotational stiffness beyond that noted with Specimen 4. Hardened steel bushings were also placed in the bolt holes, as shown in Figure 13, to reduce the elongation of the holes, increase the life of the T-section, and increase the end restraint of the connection. Specimen 4B was tested using constant amplitude loading at 116 kN (26 kip) for 2,074,000 cycles, then the load was increased to 125 kN (28 kip). At 3,140,000 cycles, a 87-mm (3.5-in) crack developed above the first bolt hole, growing past the first hole, and then continuing on toward the second bolt hole, as shown in Figure 22. The drilled hole and bolt DLM could not be applied to this specimen without drilling a hole in the T-section. Therefore, the bolt removal DLM was applied. The top two bolts in the connection were removed. This decreased the beam end rotational stiffness from about 19,000 kNm/rad. to about 7,500 kNm/rad. During an additional 1,436,000 cycles, the crack length increased only 3.9 mm (0.15 in). This short increase in crack length may represent a slight increase in the crack

length, but it may also represent limitations in the ability to precisely locate and measure the crack tip during the experiment.

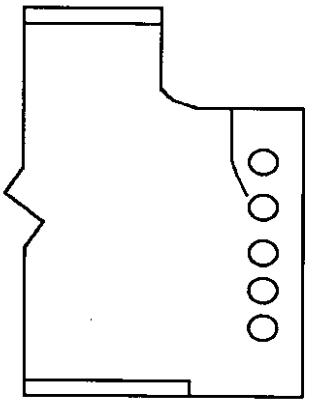

Figure 22. Specimen 4B Crack Pattern

Specimen 4 cracked at a location that limited the DLM options. Therefore, the cope of Specimen 5 was given 1.6-mm (0.06-in) deep notches at angles of 45°, 61°, and 70° from horizontal of the cope, as shown in Figure 22 and noted in Table 2. This was done to influence the crack initiation location and to hasten crack development. Specimen 5 was subject to 1.5 million cycles with constant amplitude loading at 116 kN (26 kip). The load was increased to 125 kN (28 kip). Cracking occurred in a horizontal portion of the cope, as shown in Figure 23. A second crack began as a surface crack near the first bolt hole at approximately 1,725,000 cycles, as shown in this figure. This second crack occurred only 175,000 cycles after the first crack had initiated. At 1,924,840 cycles, crack #1 was 57 mm (2.25 in) long, and crack #2 was 21 mm (0.8 in) long. Again, the crack locations did not allow the drilled hole or the inserted bolt DLMs; therefore, the bolt removal DLM was applied by removing the top bolt. This decreased the rotational stiffness by about 25 percent and the nominal cope stress by about 15 percent. Following an additional 72,800 cycles, crack #1 grew 30 mm (1.2 in) while crack #2 grew 3 mm (0.1 in). A second bolt was removed, decreasing the spring stiffness to about 50 to 60 percent of its original value, and the nominal cope stress varied between 25 and 50

percent of its original value. Testing was continued to 3,170,772 cycles at 125 kN (28 kip) and 134 kN (30 kip). At the completion of the test, the apparent crack growth for the first crack was 2 mm (0.08 in) and for the second crack was 3 mm (0.12 in).

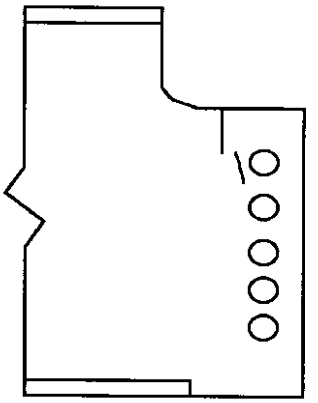

Figure 23. Specimen 5 Crack Pattern

The depths of the notches were greater for Specimen 6 and subsequent specimens, and the notches were placed at 32° and 62° from horizontal. The two notches were sharpened by drawing a blade over the tip of the notch. Specimen 6 was subject to constant amplitude loading at 116 kN (26 kip) and initial cracking occurred from the lower notch after 75,000 cycles. The crack grew vertically downwards. At 242,900 cycles, the crack was 33 mm (1.3 in) long, and a 21-mm (13/16-in) diameter hole was drilled in the beam, centered 4 mm (.15 in) below the visible crack tip. A 19-mm (3/4-in) strain gauged bolt was then inserted into the hole and tightened to a calibrated load by using a load-indicating washer that caused a load on the bolt in the range 110 to 140 kN (24.5 to 31.5 kip). The load-indicating washer was placed under the head of the bolt, and an ordinary hardened steel washer was placed under the nut. The load-indicating washers had been calibrated in previous tests to provide an additional measure of the bolt force as a function of the deformation of the washer. The strain gauged bolt did not perform reliably, and so the bolt force information is based primarily on the deformation of the load-indicating washer, and no information is available regarding the variation of

this bolt force during the test. A potentiometer was attached to the web of the beam to measure the opening and closing of the crack. At 901,700 cycles, a crack was found in the load-indicating washer under the bolt head, and it was located right over the crack in the web. The bolt was removed from its hole, and inspection showed that the hardened washer under the nut had also cracked. Two hardened washers were placed on each side of the beam web, and the test was continued. The testing was stopped at 2,188,000 cycles. A crack at the top of the inner washer on the backside of the beam was found. All washer cracks developed over the existing crack from the beam cope even though the potentiometer was unable to detect significant crack opening. The outer hardened washers used in the DLM were not cracked, nor were any further cracks noted on the beam itself.

Specimen 7 had two notches similar to Specimen 6 at 30° and 45° from the horizontal, and it had an applied nominal force of 116 kN (26 kip) for the whole test. A crack from the bottom tip of the 30° notch initiated at about 25,000 cycles and grew vertically to a length of 30 mm (1.2 in) by 80,200 cycles. A 23-mm (13/16-in) hole was drilled in the beam centered 1.6 mm (.06 in) below the visible crack tip. A normal 19-mm (3/4-in) A325 bolt was inserted and tightened, since the strain gauged bolt used in Specimen 6 did not give any meaningful information. The bolt had hardened washers under both the bolt head and the nut, and it was tightened by the turn of the nut method. Cracks in both hardened washers were noted at 561,000 cycles. The washers were not changed, but testing was continued. No new cracks were observed from the drilled hole. A second crack developed from a horizontal portion of the cope at about 1,500,000 cycles. This crack was near the stringer connection bolts, and the drilled hole and inserted bolt DLM could not be applied at this new crack location. Therefore, the test was continued, and this second crack grew to a length of 111 mm (4.5 in) by the end of the test at 1,715,000 cycles.

Specimen 8 was notched like Specimen 7, but a load of 107 kN (24 kip) was used to increase the time until initiation of cracking over that noted in Specimen 7. Specimen 8 had a crack that formed out of the lower notch at about 5,000 cycles at 30° from the horizontal. At 75,500 cycles the crack measured 22 mm (0.875 in). It was allowed to grow to a length of 37 mm, which is slightly longer than previous cracks. The crack grew too close to the connection with the T-section preventing testing of the drilled hole and inserted bolt DLM, so the bolt removal DLM was used. Since the crack did not extend to the first bolt hole, only the top bolt was removed. This resulted in only a slight reduction in the cope stress and spring stiffness, and as a result, the crack grew to 52 mm (2 in) after approximately366,000 more cycles. The second bolt was removed, and the stiffness was reduced by 35 to 100 percent from the original. The nominal stress at the cope experienced similar reductions. The load was increased to 116 kN (26 kip), and the final crack length after 2,376,480 cycles at the end of the test was 65 mm (2.6 in). The additional crack growth that occurred once the second DLM had been applied was 13 mm (0.5in).

Specimen 9 was also notched like specimens 7 and 8, but a new T-section was used because of the reduced connection stiffness due to the T-section deterioration during testing of Specimen 8. The initial loading of 98 kN (20 kip) caused a 12-mm (0.5-in) crack from the 35° notch at 80,000 cycles. The crack length was 36 mm (1.4 in) at 114,200 cycles. The 21-mm (13/16-in) hole was drilled 2.4 mm (0.1 in) vertically below the visible crack tip. A 19 mm (3/4 in) bolt was proof-loaded into the hole. The flat washers cracked at 418,000 cycles. The load was increased to 107 kN (24 kip). A crack developed from the bolt hole initiated at 1,590,000 cycles and was 86 mm (3.5 in) long at 1,729,700 cycles.

Specimen 10 was notched like specimens 7, 8, and 9, and a new T-section was used because of deterioration in stiffness noted at the end of testing of Specimen 9. The initial loading of 98 kN (22 kip) caused a 6.75-mm (0.25-in) crack at 155,000 cycles at

the 35° notch. The crack grew to 30 mm (1.2 in) with an additional 78,300 cycles, and the top bolt was removed. The removal of this bolt reduced the spring stiffness by 35 percent, and the nominal stress at the cope was reduced by a slightly greater amount. The crack was allowed to grow to a length of 128 mm (5.1 in) at 2,652,000 cycles.

Specimen 11 had the same cope preparation as Specimen 10. The initial loading of 98 kN (22 kip) caused a 13-mm crack at 92,600 cycles. The crack grew to 30 mm (1.2 in), and the two top bolts were both removed. This was similar to Test 4B, except that the crack length was shorter. The beam sustained an additional 1,029,300 cycles at 98 kN (22 kip) following the application of the DLM without crack growth. The load was increased to 107 kN (24 kip) at 1,155,890 cycles, and the bottom three bolts in the connection were replaced with new A325 bolts to stiffen the connection as much as possible for the bolt geometry. The beam underwent an additional 770,725 cycles at 107 kN (24 kip) before the load was increased to 142 kN (32 kip). A crack developed from the second bolt hole and continued to the third bolt hole. The third bolt from the top of the end connection was removed, and another crack was seen beginning to the left of the third bolt hole, growing towards the fourth hole. The first crack was 53 mm (2.1 in) and the second was 44 mm (1.7 in). The crack from the notch exhibited no growth after the initial DLM. The test was ended after a third crack developed. All five bolt holes measured after test completion showed no signs of elongation.

Specimen 12 had the same notch pattern as specimens 7 through 11. There was also a flaw in the horizontal portion of the cope above the bolts. Initial cracking from the flaw in the beam occurred at 200,000 cycles. The 53-mm (2.1-in) crack was noticed at 287,000 cycles. The bolt removal DLM was applied, and the top three bolts in the end connection were removed. This bolt removal reduced the spring stiffness by approximately 35 percent, but the initial stiffness was significantly smaller than most earlier specimens. The beam was loaded at 98 kN (22 kip) for an additional 1,009,500 cycles after the DLM was applied, and no additional crack growth occurred. The load

was systematically increased to 125 kN (28 kip). This test showed no crack growth beyond the initial 53 mm (2.1 in) for 2,406,260 cycles after the DLM had been applied. The test was ended at 2,694,059 cycles.

EVALUATION OF FATIGUE BEHAVIOR AND DAMAGE LIMITATION METHODS

The previous chapter briefly summarized the tests completed in this research program. This summary provides a basic understanding of this important research problem, but variations occurred in each test because of slight differences in the test specimens or wear and deterioration of the test apparatus. Therefore, the summary is less definitive than desired. Additional analysis, evaluation, and comparison of the test data is required to fully understand the consequences of these test results. These evaluations are provided in this chapter.

EVALUATION OF CRACK INITIATION

Regular and frequent inspections were completed to determine initiation of cracking. For all test specimens in this study, initiation of cracking was defined as the point when visible cracking was first noted during these regular inspections. The frequency of these inspections was increased at times when crack initiation was expected. As a result, the length of a crack at first observation was generally less than 5 mm (0.2 in), but cracking occurred unexpectedly for several specimens, and somewhat longer initial crack lengths were possible with these specimens. In all specimens except Specimen 4, cracking did occur, and several specimens experienced multiple initiations. Multiple initiations occur when two cracks begin at different locations on the same specimen. The hole drilling and inserted bolt DLMs require drilling a hole through the tip of the crack, and development of a crack out of the drilled hole also constitutes an initiation. Lengthening of existing cracks is not considered a crack initiation. The total number of load cycles until initiation, N_{eff}, the load at crack initiation, and the effective stress, σ_{eff}, to crack initiation are provided in Table 3. This effective stress was computed

for the total number of load cycles at the location of crack development in the cope according to Equation 2, and the nominal effective stress at the critical cope location was defined in Equation 9. This stress is strongly dependent on k_s. The initial cope condition and location(s) of crack initiation are also noted in the table.

Table 3. Initial Cracking for All Tests

(1) Test No.	(2) Total No. of Cycles	(3) Load (kN)	(4) σ_{eff} (MPa)	(5) Initial Cope Condition	(6) Location of Crack Initiation
0A	385,000	89	47.64	Square Cut	Near Corner of Cut
0B	980,000	82	47.45	Square Cut	Near Corner of Cut
1	1,675,000	146	89.71	22mm radius Smooth Cope	Cope Radius Meets Horizontal Part of Cope
2	450,000	123	108.3	22mm radius Smooth Cope	Cope Radius Meets Horizontal Part of Cope
3	3,672,500	120	75.27	22mm radius Smooth Cope	Slightly left of the line of bolts at the cope
3B	2,050,000	107	86.91	22mm radius Smooth Cope	Cope Radius Meets Horizontal Part of Cope
4	-	-	-	22mm radius Smooth Cope	No Crack seen
4B	3,102,100	120	76.94	22mm radius Smooth Cope	Slightly left of the line of bolts at the cope
5	1,550,000 -1st Crack	115	78.69	22mm radius Cope with three 1.6mm notches at 45, 61, & 70 degrees	Slightly left of the line of bolts at the cope
	1,725,000 -2nd Crack	120	79.64	22mm radius Cope with three 1.6mm notches at 45, 61, & 70 degrees	2nd Crack – originates from 1st bolt hole, not connected to 1st crack
6	75,000	60	74.78	22mm radius Cope, two 3.0mm sharp notches, 32 & 62 degrees	At base of 32 degree notch
7	25,000 - 1st crack	123	100.79	22mm radius Cope, two 3.0mm sharp notches, 32 & 62 degrees	At base of 30 degree notch
	1,500,000 -2nd crack	110	60.73	22mm radius Cope with two 2.5mm sharpened notches at 30 & 45 degrees	Slightly left of the line of bolts at the cope
8	5,000	87	96.71	22 mm radius Cope with two 2.5mm sharpened notches at 30 & 45 degrees	At base of 30 degree notch
9	50,000 - 1st crack	104	113.24	22mm radius Cope with two 2.5mm sharpened notches at 35 & 45 degrees	At base of 35 degree notch
	1,590,000 crack redevelops	106	71.06	22mm radius Cope with two 2.5mm sharpened notches at 35 & 45 degrees	Lower right portion of bolt hole used in DLM
10	150,000	101	89.6	22mm radius Cope with two 2.5mm sharpened notches at 35 & 45 degrees	At base of 35 degree notch
11	50,000 - 1st crack	106	31.41	22mm radius Cope with two 2.5mm sharpened notches at 35 & 45 degrees	At base of 35 degree notch
	1,955,000 –2nd crack	136	14.38	22mm radius Cope with two 2.5mm sharpened notches at 35 & 45 degrees	2nd bolt hole in End connection
12	200,000	102	83.22	22mm radius Cope with two 2.5mm sharpened notches at 35 & 45 degrees	At Flaw in horizontal portion of cope

The relative effectiveness of the cope detail at delaying the initiation of cracking can be seen in Figure 24. Here it can be seen that the specimens with the square-cut cope (specimens 0A and 0B, represented by the dark squares) and those with notched flame cut copes (specimens 5, 6, 7, 8, 9, 10, 11 and 12, represented by the dark diamonds) lay below the Category E' S-N curve. Cracking initiated in these specimens very rapidly because of the roughness and sharp corners of the cope region. The geometry caused stress concentrations and introduced flaws that served as a ready source for crack growth. The figure shows that Specimen 5 had a longer life than the other ones, and this may be because of the notch in this specimen was not sharpened before testing.

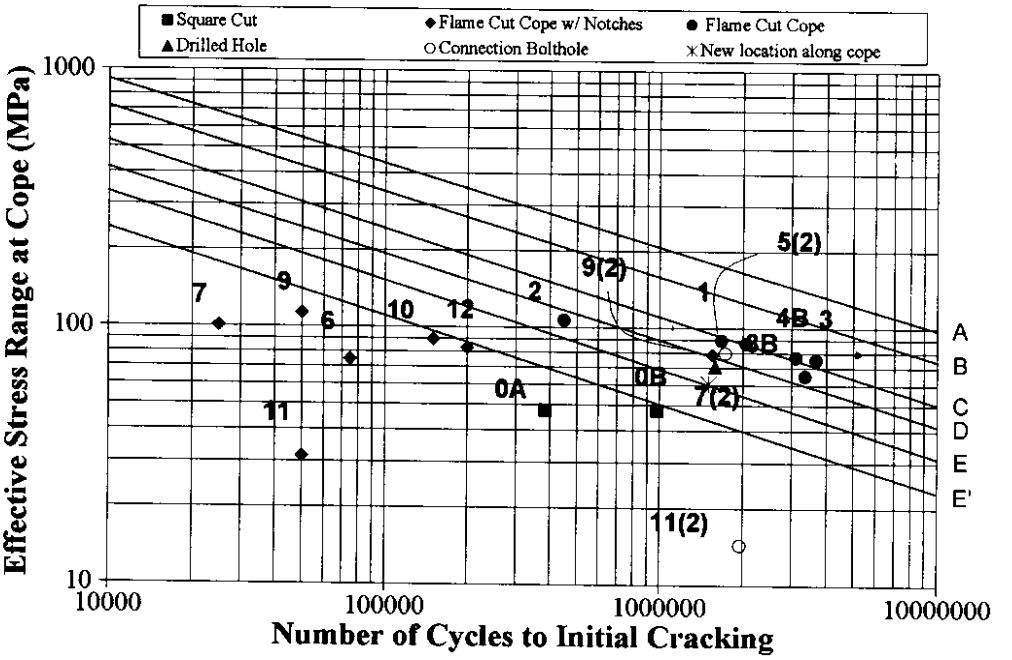

Figure 24. S-N Curve: Initial Cracking of Specimens

The flame cut copes of these test specimens were intended to simulate the actual detail in the prototype bridge. However, the laboratory flame cut copes were made with a template, and comparison of the finish of these cuts to those noted in the prototype

structure showed that the prototype connections were probably closer to the notched cope detail than to the flame cut cope detail. Figures 3 and 25 are photographs of copes from WSDOT bridges. Comparison of these photos with the specimens tested in this study indicated that the photographed copes clearly qualified as rough or notched cope details. Therefore, cope details such as these will crack at relatively few cycles of relatively low stress range.

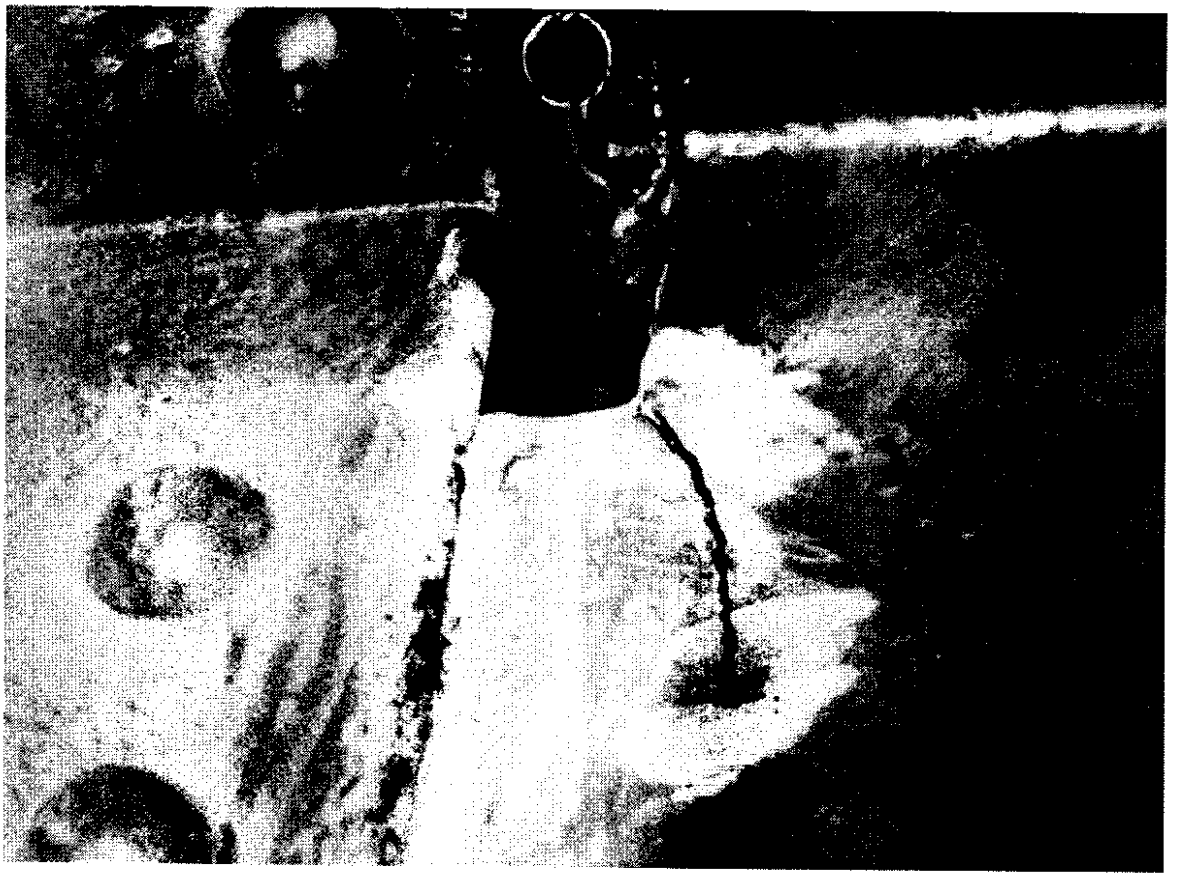

Figure 25. Photograph of a Coped Stringer Connection

Several specimens had multiple cracks, and these multiple cracks are identified by a sequence number in parenthesis in Figure 24. These second cracks invariably occurred

outside of the notches in the cope. The figure shows that fatigue cracks that occurred outside the notched area or in flame cut copes without a notch generally required a much longer time to initiate visible cracking. There is clear scatter in these results, but flame cut copes with surface conditions such as noted in these specimens and summarized in Table 2 are likely to initiate cracking no sooner than Category E and no later than Category C. On average, these flame cut copes are likely to initiate cracking around the Category D S-N curve.

Several cracks initiated out of drilled holes. In some cases the drilled hole was used as a DLM, and in other cases the crack developed from a hole that was left open after removal of a bolt. The figure indicates that the cracks developing from these bolt holes required a length of time similar to that noted for the flame cut coped connections. The second crack of Specimen 11 was an exception to this observation, but all cracking on Specimen 11 occurred exceptionally early, as noted in the figure.

There is considerable scatter in the initial cracking test results. This is commonly noted with fatigue experiments because of the influence of flaws that are not apparent in the initial test specimen but that clearly affect the results. The scatter is particularly large for the notched coped specimens, and this suggests that a small difference in notch characteristic can have a significant effect on fatigue life. It also suggests that smoothing the cope and polishing the cope region before initiation of cracking may greatly extend fatigue life. It should be noted that initiation of fatigue cracking is an issue of concern, but it is clearly not the end of the fatigue life since considerable time is sometimes required for the crack to grow to a size of major concern.

CRACK GROWTH

Once a crack has visibly initiated, the rate of crack growth becomes important. Once a visible crack has initiated, further crack growth will occur. The State II elastic crack growth model described in equations 3 and 4 and figures 9 and 10 of Chapter 1

model this crack growth behavior. By this theory, the rate of crack growth can be empirically monitored for a given connection (or group of identical connections). These data should then be plotted in the form of Figure 9, and the coefficients, C and n, are determined by an empirical curve fit to the data. The coefficient, n, is determined by the slope of the straight line fit to the data on the log-log plot, and C is determined from the apparent intercept of this straight line at a stress concentration factor of 1.0. A number of tests included in this research were evaluated by this method [Skare 1999]. This evaluation was not successful in developing a predictive method. Coefficients were computed, but very different coefficients were predicted by nominally identical tests. Furthermore, none of the computed coefficients provided realistic predictions of crack growth rates in other specimens. As a result, this evaluation is not described in this report.

There are several reasons why this theoretical model was not successful. First, the theory is based upon an idealized state of stress and crack development, while the coped stringer-to-floorbeam connection has a complex state of stress with sharp changes in geometry and stress gradients. Second, the change in crack length has be to accurately measured for empirical development such as illustrated in Figure 9. Location of the tip of the crack is difficult to determine, and small errors in crack length measurement can translate into large errors in the calculation of change in crack length. Finally, the theory also requires the determination of a stress intensity factor, ΔK (see Equation 3 and Figure 10). The factor ΔK is never determined with great accuracy even under ideal circumstances, but the stress state in the coped stringer connection is far from ideal, and this estimated concentration factor is very uncertain.

Although the elastic crack growth theory is not productive, the situation is not hopeless. Application of the basic concepts of the theory can provide a general understanding that leads to at least an approximate method for evaluating the fatigue life

remaining after initiation of cracking. Once a visible crack is present, the crack growth rate depends upon the global geometry of the specimen, the state of stress, and the crack length. That is, once a crack has become visible, the stress intensity and the rate of crack growth should not depend upon the notches in the connection or the initial surface finish of the cope. The global geometry of the test specimens were all identical and were consistent with the stringers and connections used in the steel truss bridges. As a result, the above observation has dual consequences. First, it means that the number of cycles necessary to cause a specific increase in crack length should be approximately the same for all specimens that have the same stress state. Second, connections with a relatively smooth initial finish will require many cycles to initiate cracking, but the number of cycles required to lengthen the crack a specific amount will appear relatively short in comparison to initial crack initiation period. With rough or notched cope details, the number of cycles required to initiate cracking is short in comparison to the time required to initiate cracking in smooth coped surfaces. As a result, the number of cycles required to lengthen the crack a specific amount will appear relatively longer for connections with rough cope regions. This heuristic argument is supported by the data presented in Table 2.

Specimens 2, 8, and 9 all had effective stresses of approximately 100 MPa (14.5 ksi), and they progressed from crack initiation to approximately a 30-mm (1.2-in) crack in 57, 85, and 64 thousand cycles, respectively. These numbers are quite comparable, although the initial finish of the copes varied widely for these specimens. Furthermore, the time required to initiate visible cracks varied by more than an order of magnitude for these specimens. Similar comparisons can be made for other connections, other stress levels, and other crack lengths. The comparisons are never exact, but they generally support the above hypothesis.

As a potentially useful application of this concept, the number of cycles and stress range required to develop a 50-mm (2-in) crack was selected. This crack length was

selected because there were a significant number of data points for this prediction, and it is a length that will be regarded as serious by many engineers. Most specimens' cracks were not have crack measured at precisely at 50 mm. Other specimens (particularly those with removed bolts) did not develop cracks to a full 50 mm. To maximize the data available for this comparison, the number of cycles for these specimens were linearly prorated to an estimated 50-mm crack length. Crack growth is not linear, and the linear approximation may either underestimate or overestimate the number of cycles required to develop this selected crack size, but the inaccuracy should not be large because the crack length is still quite short in comparison to the dimensions of the specimen. Figure 26 shows the effective stress range as a function of the number of cycles required to develop the 50-mm (2-in) crack after crack initiation. Since the prorated data are more approximate, they are noted as solid squares while other data are noted has hollow squares. In general, the data appear to fit together in an appropriate manner. Furthermore, the AASHTO S-N curves are plotted on this same figure to lend perspective to the relative magnitude of the data points. The S-N curves have no meaning for this curve beyond that relative comparison. It can be seen that the data fall into a more or less straight line, and the average number of cycles required to develop this 50-mm (2-in) crack length falls consistently below AASHTO Fatigue Category E'. A least squares regression to these data was completed, and a curve that was two standard deviations below the mean was selected as a conservative indicator of the number of cycles expected after initiation of visible cracking but before the development of a 50-mm crack. The resulting equation was

$$N = \frac{5.4\ 10^{10}}{S_{eff}^{3}} \qquad \text{(Eq. 12)}$$

This estimate is conservative in that approximately 97.5 percent of comparable specimens should require a longer number of cycles for crack development, given the effective stress at the critical region of the coped specimen.

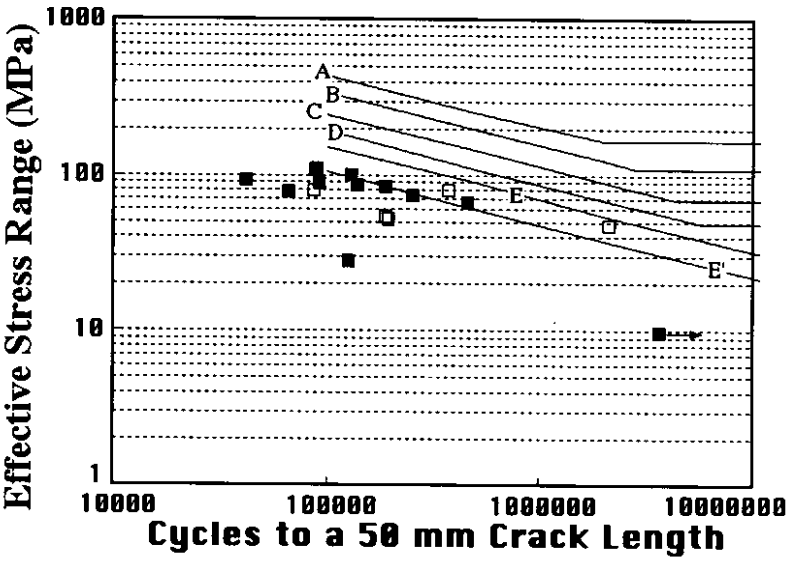

Figure 26. Number of Cycles Required to Develop a 50 mm Crack

DLM EFFECTIVENESS

The previous discussion considered the effective stress range and number of cycles required to initiate a visible crack and the subsequent cycles needed to develop the crack to a significant length. Once the crack has attained a significant length, damage limitation methods offer the only significant alternatives to replacement of the bridge stringers and connections. This research showed considerable variation in the effectiveness of different DLMs, and so a comparison and evaluation of the relative effectiveness of the various alternatives is provided here.

No DLM

If no DLM is employed, then the crack will continue to grow, and the tests suggest that the crack will tend to grow toward the bolt group. This is consistent with the shear force diagram and with direct fatigue cracks seen in stringers of actual bridges such as the Lewis River truss bridge. While some cracks have been observed to continue horizontally beneath the top flange, these cracks are most commonly seen in members subject to deformation fatigue, such as the floor beams of the Toutle River tied-arch

bridge[Roeder et al 1998]. If a crack would grow away from the cope into the beam, it would grow toward the point of contraflexure. Near the point of contraflexure, the demands would be much less, decreasing the crack growth rate.

As the crack grows it reduces the spring stiffness at the end of the beam, but since limited deformation occurs across a small crack, this stiffness reduction is often very small. If k_s is reduced sufficiently, the stress at the crack tip will become compressive, restricting further crack growth. However, this did not happen in any of the tests completed during this study because relatively small changes in k_s were noted with increasing crack length. Fortunately, the crack growth was slow and stable, but the growth rate increases as the crack grows longer. The relatively slow, stable crack growth rate means that there is time to discover a crack before it causes a serious problem. However, the crack growth does not appear to stabilize, and so something must ultimately be done to control the crack growth. That is, a DLM must be applied to control further crack growth, the loads on the stringer must be limited to reduce the effective stress and control the crack growth, or the damaged member and connection must be replaced.

Hole Drilling Method

This method was used with specimens 2 and 3B. Specimen 2 required 450,000 cycles of loading to initiate the first visible crack and an additional 57,000 cycles for the crack to grow to 32 mm (1.25 in) at a relatively stable effective stress limit. A 22-mm (7/8-in) hole was drilled as a DLM for this specimen, and the crack reinitiated and grew to an effective total length of approximately 50 mm (2 in) after an additional 70,000 cycles. If the crack had been allowed to grow without application of the hole drilling DLM, this additional crack growth would have required only 20,000 to 40,000 cycles. Thus, the hole drilling DLM benefited the connection performance. However, the first crack initiation required 450,000 cycles at the given effective stress level. The hole drilling method effectively removes the crack tip and theoretically returns the specimen

to nearly an original surface condition. Thus, the expectation was that the hole drilling DLM would allow at least 200,000 to 300,000 cycles before a new crack initiated and lengthened to the specified length. The tests showed that the hole drilling DLM reduced the rate of crack growth, but the reduction was much smaller for these coped stringer connections than would be suggested by elementary crack growth theory. A second drilled hole was used for this specimen, and a third crack initiated from that hole with a sequence of events similar to that noted for the second crack.

On Specimen 2, a hole was drilled that was consistent with the procedure commonly used in WSDOT practice. Specimen 3B was tested with a somewhat larger drilled hole, since this larger hole radius was expected to reduce the stress concentrations and delay the potential for cracking. This specimen required 2,050,000 cycles for initiation of visible cracking, and 103,000 additional cycles to lengthen the crack to 27 mm (1.1 in). A 31.7-mm (1 1/4-in) hole was drilled through the crack tip, and a new crack then developed and lengthened to an additional 25.4 mm (1 in) in 247,000 cycles at the same stress level. Specimen 3B had a larger diameter hole and a smaller effective stress than Specimen 2, and so cracking developed more slowly in Specimen 3B than in Specimen 2. In both cases the hole drilling DLM allowed a longer time before crack reinitiation than would be allowed if no DLM were applied, but the increased number of cycles was much smaller than would be expected if the DLM had fulfilled its stated objective. The drilled hole DLM extended the life of specimens 2 and 3B only an estimated additional 70,600 to 192,000 cycles. This increase is relatively small in comparison to the number of cycles required to initiate the first crack. Note that special care was taken in the laboratory to capture the end of the crack by polishing the area and by using dye penetrant. In an actual structure that is deforming and deflecting under traffic during inspection, and where inspection access may be difficult, the possibility of finding the tip of the crack is much less likely than in the laboratory. This represents a further limitation of the method.

Hole Drilling and Bolting Method

The drilled hole with inserted bolt DLM was used on specimens 6, 7, and 9, and several key observations of the behavior noted during these tests are summarized in Table 4. Three types of behavior were found after the DLM was applied. Specimens 6 and 7 exhibited no further crack growth from the initial crack. In this sense, the drilled hole with inserted bolt was a very effective DLM. While Specimen 7 exhibited no further crack growth at the initial crack, another crack developed at another location. This raises a key concern with all DLMs. A DLM may be very effective in preventing further crack growth at the initial crack location, but the flame cut, riveted, coped stringer connections have multiple sources of flaws in the region of the cope, and additional cracks may occur in the rivets or in other sources of the connection. The drilled hole with inserted bolt DLM may be particularly sensitive to that problem, because this DLM does not significantly reduce the spring stiffness of the connection, and the effective stress in the coped region remains relatively large within the critical cope region after the DLM is applied. Table 4 shows that the drilled hole with inserted bolt DLM dramatically extended the fatigue life of Specimen 9, but eventually cracking initiated and grew from the existing hole. The crack initiated very slowly in the existing hole, since the number of cycles required to develop a significant crack was approximately 15 times as large as the number of cycles needed to develop the initial crack. Therefore, the drilled hole and inserted bolt DLM was considered to be effective in all specimens, but it clearly did not prevent all further cracking. In all tests the washers between the web and the bolt head and between the web and the nut cracked above the original crack before additional damage was noted in the beam web. This suggests that washers at these locations can be used to provide warning before any further crack growth. The cracked washer provides an excellent warning system for inspectors. After it is discovered, new washers and a new bolt can be inserted, although it is not clear how effective replacement bolts and washers will be after multiple replacements. Note, however, that cracks growing out of drilled

holes with an inserted bolt progress very rapidly once the crack has initiated, and there appears to be less time and warning regarding this crack growth than with other DLM methods.

Table 4. Specimens Using Hole Drilling and Bolting DLM

Specimen	6	7	9
Before DLM Applied			
Effective Stress	73.5 MPa	88.6 MPa	109.91 MPa
Crack length/	33 mm	30 mm	36 mm
No. cycles	243,052	80,231	114,329
After DLM Applied			
No. cycles	2,188,401	1,715,100	1,729,710
Crack length	No growth	No growth of original crack New crack 111 mm	Crack growth of 86 mm

Bolt Removal Method

Bolt removal from the end connection was the DLM used with specimens 4B, 5, 8, 10, 11, and 12. Specimens 4B and 11 tested the effect of removing two bolts simultaneously, and specimens 5 and 8 tested the effect of removing a total of two bolts one at a time. Specimen 10 studied the effect of the removal of only one bolt, and Specimen 12 studied the effect of removing three bolts from the end connection. Table 5 summarizes some critical data from these tests. Removal of one bolt was not sufficient to stop cracking for any specimen. This may have been because the crack length was similar to the distance between the top of the cope and the first bolt hole before the top bolt was removed. There was also a very limited reduction in k_s with removal of a single bolt. Removal of two bolts severely slowed the cracking of the original crack. In the worst case, the crack length slowed to 39 mm in 1.9 million cycles. This type of retrofit may be satisfactory for many structures. In the best cases (specimens 4B and 5), the increased crack length observed during more than a million cycles was small enough that it could

easily be attributed to uncertainty in the measurements of the initial crack length rather than a significant growth of the crack. However, care must be taken that additional new cracks do not occur as they did in Specimen 11. Removal of three bolts was very effective for the specimen tested.

Table 5. Specimens Using Bolt Removal DLM

Specimen	4B	5	8	10	11	12
Before Bolts Removed						
k_s (kNm/rad.) - initial	19,500	19,500	≈27,500	≈27,600	9,100	16,000
Crack length/ No. cycles	87 mm 3,140,187	57 & 21 mm 1,924,000	37 mm 102,070	30 mm 233,683	30 mm 126,622	53 mm 288,000
Bolt #1 Removed	-				-	-
k_s (kNm/rad.)		12,800	16,000	16,000		
$k_s / k_{s,initial}$		66%	58%	58%		
Crack length/ No. cycles		+3 & 30 mm +72,800	+14.6 mm +365,950	+3 mm 1,607,600		
Crack length/ No. cycles		-	-	+129 mm 2,417,900		
Bolt #2 Removed				-		-
k_s (kNm/rad.)	8,500	8,500	6,000		0	
$k_s / k_{s,initial}$	44%	44%	22%		0%	
Crack length/ No. cycles	+ 4 mm +1,435,900	+2 & 3 mm +1,173,100	+39 mm +1,908,280		Existing– none +263,400	
Crack length/ No. cycles	-	-	-		New- +96 mm +263,400	
Bolt #3 Removed	-	-	-	-	-	
k_s (kNm/rad.)						0
$k_s / k_{s,initial}$						0%
Crack length/ No. cycles						+ None +2.41m

The effectiveness of the bolt/rivet removal DLM results from the decrease in stiffness of the end connection. The method does not prevent further crack growth. It simply reduces the effective stress at the crack so that it is less likely to lengthen. Table 5 shows that removal of a single bolt reduces k_s by 30 to 45 percent, and this has a limited benefit in retarding further crack growth. Removal of two bolts reduced k_s to less than 44 percent of the initial value (sometimes as low as 0.0), and this significantly retarded further crack growth even at a relatively large applied load. If k_s and σ_{eff} were reduced to 0.0, no further lengthening of the cracks was noted. Equation 12 will provide a conservative estimate of the number of cycles needed to develop a 50-mm crack as a function of σ_{eff} for conditions in which the 0.0 stiffness goal is not achieved. If the decrease in stiffness can be predicted, application of an appropriate DLM becomes less of an art and more of a science. Further discussion of this is provided in the next chapter.

PRACTICAL CONSEQUENCES OF RESEARCH RESULTS

GENERAL STRATEGY

This report considers fatigue cracking of the riveted, coped stringer-to-floorbeam connections that are commonly used in truss bridges in Washington State. Laboratory experiments were performed on these connections to evaluate the fatigue cracking and possible DLMs for the connection. The fatigue cracking is caused by the stress induced by negative bending moments that result from the rotational restraint or k_s of the connection.

Previous chapters summarized and evaluated the research results. The experiments showed that visible fatigue cracking initiates much more quickly with rough or notched cope details, which are common on many WSDOT bridges. The effective stress, σ_{eff}, computed by Equation 2 will typically fall well below the Category E' S-N curve when the initiation of visible cracking occurs from these rough and notched cope details. With smoother flame cut copes that have no notches and surface roughness in the range ST250, a much longer period of time is required to for visible cracking to initiate. The research showed that, on average, cracks will initiate from these details when σ_{eff} reaches the Category D S-N curve. This time period can be orders of magnitude longer than that required to initiate visible cracks with the notched and rough cut details. Therefore, one obvious and effective way of upgrading existing cope details is to improve the surface and finish of the existing cope. While this alternative will be very effective, it may be of limited practical value because there are so many of these cope details on the steel truss bridges, and they are relatively inaccessible for finishing work. As a consequence, other alternatives are needed.

One alternative is to do nothing. This research examined the time required for the crack to grow to a significant length. Normal elastic crack growth theory was examined, but this theory was ineffective in providing practical guidance because of the complexity of the geometry and stress state in the coped stringer-to-floorbeam connection. As a result, an empirical model that is heuristically consistent with linear crack propagation theory was developed. Equation 12 provides an estimate of the number of stress cycles as a function of σ_{eff} required to increase the crack length from an initially visible condition to a significant length. A significant length, l_{eff}, was defined as 50 mm (2 in) for the test specimens, but this significant length will be affected by the scale of the specimen. The test specimens were moderately large scale, but the effective length will be longer with deeper stringers. Therefore,

$$l_{eff} = \frac{d_b}{10.5} \qquad \text{(Eq. 13)}$$

where d_b is the beam depth. Equation 13 will result in a crack length estimate in mm if the depth is in mm and inches if the depth is in inches. The number of cycles, N, predicted by Equation 12 to develop this crack length is two standard deviations below the mean. Thus, approximately 97.5 percent of specimens with initial visible cracking will require a larger number of cycles and a resulting longer period of time for this crack growth. It must also be emphasized that this estimate is only for the geometry evaluated in this study. Figure 27 illustrates the limitations of this geometry and the method.

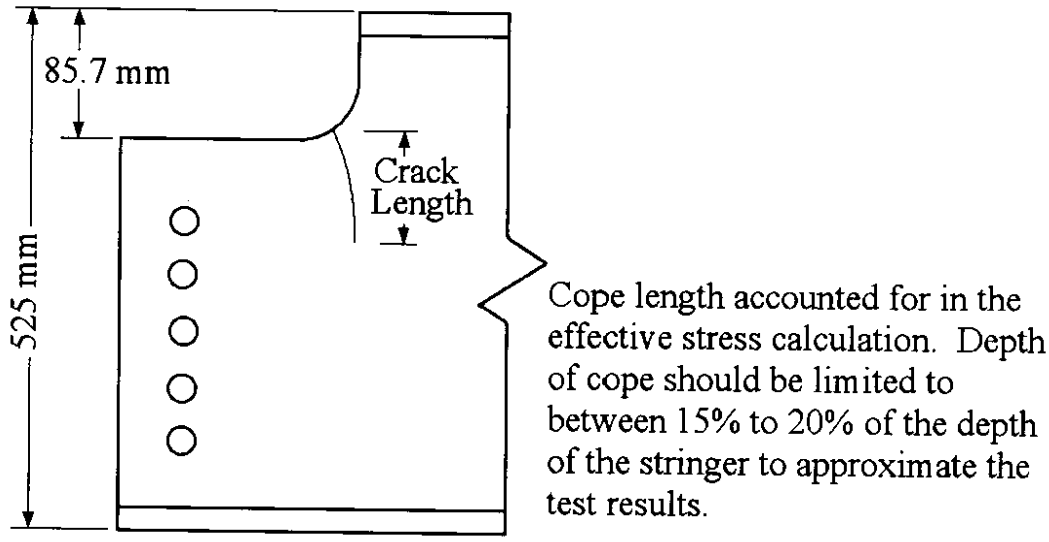

Figure 27. Limitations of the Empirical Crack Growth Estimate

The number of cycles (and time) predicted by Equation 12 will appear moderately long in comparison to the number of cycles required to develop initial visible cracking with notched or rough flame cut copes, but it will appear moderately short in comparison to the number of cycles required to initiate visible cracking for smooth cope details. Depending upon the magnitude of σ_{eff} and the daily volume of truck traffic on the bridge, Equation 12 may show a significant period of time for the crack to grow to a significant length. If σ_{eff} is small, no further modification may be needed if the bridge receives regular inspections to monitor the crack growth. However, DLMs may be employed to retard the crack growth in other circumstances.

The drilled hole DLM was shown to retard crack growth somewhat more than suggested by Equation 12, but the beneficial effect is quite limited. The time required for development of a crack of length, l_{eff}, appears to be about 50 percent longer than indicated by Equation 12. The drilled hole DLM falls far short of returning the specimen to an uncracked condition with a reasonably smooth cope finish. The drilled hole method is

slightly better than returning the cope to a new rough or notched cope without a visible crack. However, improvements to the performance of the hole drilling DLM could be made with better models for evaluating the stress state and crack growth from the coped connection. These improved models may lead to better methods of evaluating the required hole radius, ρ, for retarding further crack growth. As a result, the drilled hole DLM is presently believed to be of limited value for deterring crack growth, but significant improvements are possible with further research.

The drilled hole with inserted bolt DLM requires a drilled hole, and then a high strength bolt is inserted and tightened to the proof load of the bolt. The hole is drilled through the tip of the crack, and the surfaces are polished to reduce or eliminate potential flaws. This method is very effective at delaying further crack growth. This DLM may extend the remaining fatigue life to something approaching that achieved with a new cope with relatively smooth flame cut surfaces. It is recommended that hardened steel washers be placed between both the nut and the head of the bolt and the beam web. The tests showed that these washers will crack before further crack growth emanates from the drilled hole, and this washer cracking serves as a warning for periodic inspections of the stringer connections. However, this DLM has three potential concerns. First, this DLM does not reduce the spring stiffness of the connection, and so the moment at the cope and the stress at the cope remain relatively high. The high stress means that cracks are more likely to occur at an adjacent location in the cope region before the full benefit of the DLM has been achieved. Second, this DLM does not prevent all future cracking at the drilled hole. Cracks may reinitiate after many cycles, and once these cracks reinitiate, the experiments indicated that the re-initiated cracks grow somewhat more rapidly than the rate suggested by Equation 12. This can be seen by noting that the time period required for crack growth after re-initiation of visible cracking in Specimen 9 falls to the left edge

of the data in Figure 26. Third, the hardened washer serves as a fuse, indicating possible further cracking, but inspection of these washers may be difficult.

The bolt removal DLM is also very effective if the spring stiffness, k_s, and the effective stress, σ_{eff}, are reduced to a very low value. The tests suggested that the optimal goal of this DLM should be to reduce σ_{eff} to 0.0 (or into compression), since no further crack lengthening is expected if the crack cycles in compression. This DLM may not be practical for some connections because all connections have some rotational stiffness. However, it should be possible to come quite close to this goal with many practical connections. The tests showed that the maximum k_s after bolt removal should be no more than 40 percent of the original connection stiffness if the method is to be effective. A later section of this chapter will discuss methods of achieving this goal.

All of the available options for limiting this fatigue cracking require an understanding of the effective stress at the critical location of the coped region, σ_{eff}. This stress is particularly important with the bolt removal DLM and for evaluating the number of cycles required to develop significant cracking in Equation 12. The methods for establishing this effective stress level are standard analysis methods, but they are not commonly used by bridge engineers. Therefore, this chapter will address the tools available for this evaluation.

EFFECTIVE STRESS AT THE COPE OF THE STRINGER, σ_{eff}

The effective stress, σ_{eff}, is the key parameter in the evaluation process because this determines the number of cycles that a given connection can tolerate, and it establishes the effectiveness of various DLMs. The effective stress at the cope depends upon the bending moment at the cope, M_{cope}, caused by the effective truck loads on the bridge. This moment is converted to a stress at the top of the cope, σ, by dividing the

bending moment by the section modulus, S, of the reduced section, as shown in Figure 28.

$$c = \frac{\left(d_c - \frac{t_f}{2}\right) t_f b_f + \frac{(d_c - t_f)^2 t_w}{2}}{t_f b_f + (d_c - t_f)\, t_w}$$

$$S = \frac{\left(d_c - c - \frac{t_f}{2}\right)^2 t_f b_f + \frac{(d_c - t_f)^3 t_w}{12} + (d_c - t_f) t_w \left(c - \frac{(d_c - t_f)}{2}\right)^2}{c}$$

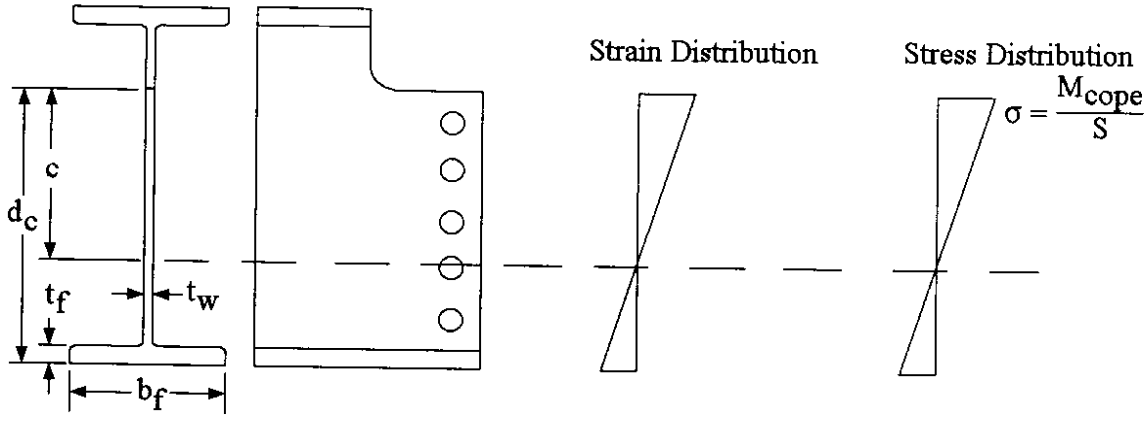

Figure 28. Geometry for Defining Section Modulus of Reduced Section

The moment at the critical location of the cope, M_{cope}, depends upon the effective load, P_{eff}, and k_s at each end of the stringer. The determination of the parameters, P_{eff} and k_s, are discussed in later sections, but given these parameters, the bending moment is determined by the indeterminate analysis of the stringer and its end connections. This analysis was discussed in Chapter 2 for the case in which the spring stiffness is applied at one end of the stringer and the other end of the stringer is pinned, as shown in Figure 15. For this case, M_{cope} is determined by Equation 9, and θ is defined by the equation

$$\theta = \frac{P}{k_s + \frac{3EI}{L}} \left\{ \frac{L_p}{2} - \frac{L_p^3}{L^2} \right\} \qquad \text{(Eq. 14)}$$

and all geometric terms are defined in Figure15. Note that L_p should be approximately 0.6L for the maximum stress range in the cope of this connection. This analysis procedure applies at the end stringer on most bridges because the end floorbeams offer little rotational resistance to the stringer.

Internal stringers have end restraint at both ends of the stringers, and the analysis procedures must be used with the geometry as illustrated in Figure 29. For this case, maximum M_{cope} is caused by the application of the effective load near the mid-span of the stringer, and M_{cope} is defined by

$$M_{cope} = P\left\{ \frac{L^2}{8\left(L + \frac{2EI}{k_S}\right)} - \frac{L_{cope}}{2} \right\} \qquad \text{(Eq. 14)}$$

where L_{cope} is the distance to the point in the cope region where cracking is anticipated, as shown in Figure 29.

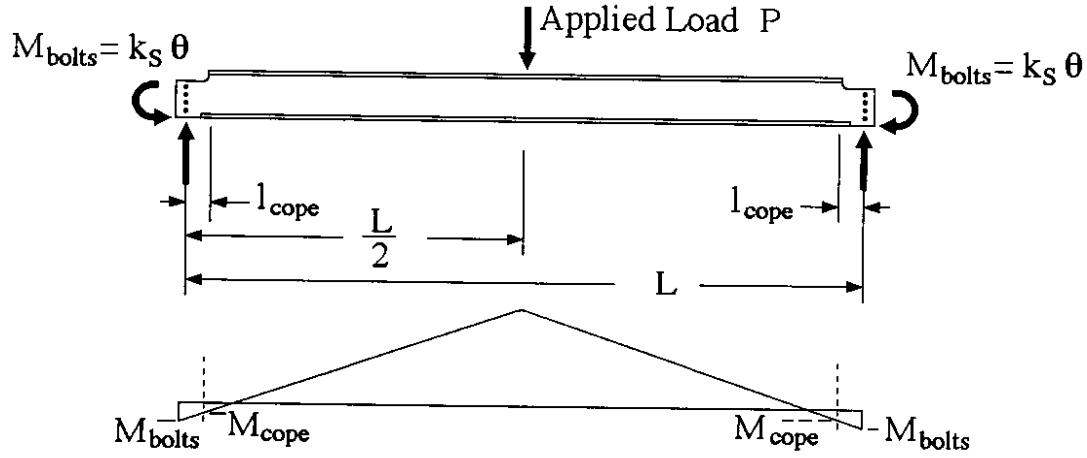

Figure 29. Geometry and Moment Diagram for Internal Stringer

SPRING STIFFNESS, k_s

The spring stiffness, k_s, is a critical parameter in the evaluation of the effective stress in all cases. A study[Kalogiros 2000] was completed to provide a method of estimating connection stiffness as a function of the number and size of bolts or rivets in a

connection. A number of connections tested by various researchers were studied to develop a relationship between connection stiffness, k_s, and the second moment of area of the bolt group, I_{bg}.

$$I_{bg} = \Sigma A r^2 = A_{bolt} \Sigma (r - r_{centroid})^2 \qquad \text{(Eq. 15)}$$

Figure 30 shows the stiffness as a function of I_{bg}. Kalogiros used a least squares fit between bolt group stiffness, k_s, and the second moment of area of the bolt group, I_{bg}, to obtain Equation 16.

$$k_s = (550 \text{x} 10^6 \text{ kN/m}^3\text{/radian}) \, I_{bg} \qquad \text{(Eq. 16)}$$

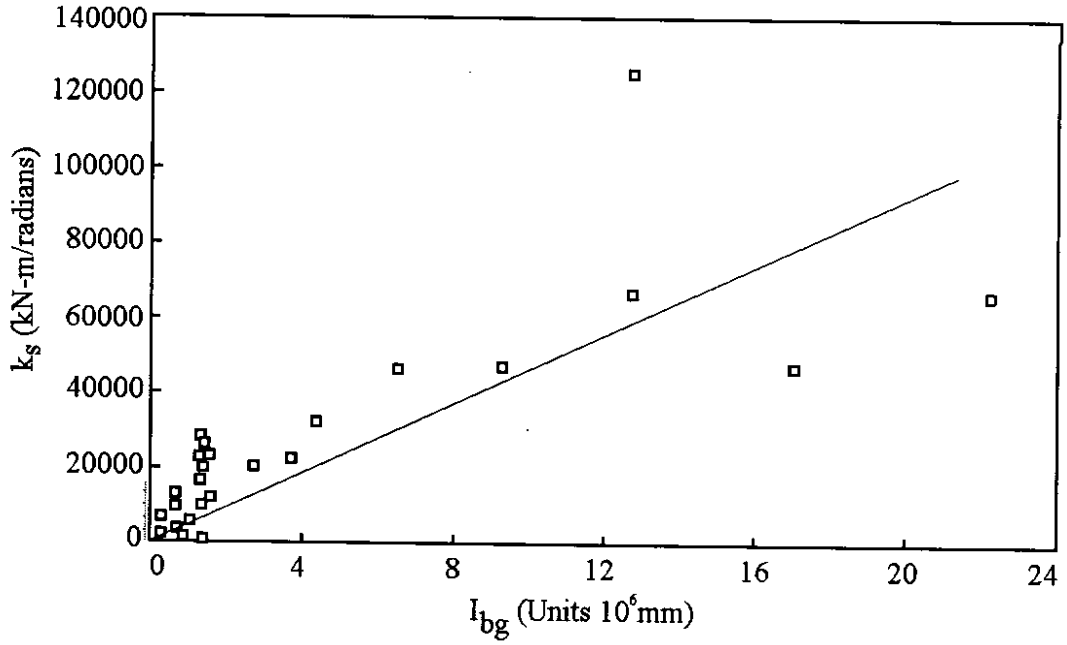

Figure 30. Measured Spring Stiffness from Past Web Angle and Shear Tab Experiments

With this formulation and five equally spaced bolts in a connection, removal of one bolt, two bolts, three bolts, and four bolts will result in a connection stiffness of approximately 50 percent, 20 percent, 5 percent, and 0 percent of the original value, respectively. If stress is proportional to stiffness, and fatigue life is proportional to stiffness cubed, then the resulting fatigue lives will be 8 times, 125 times, 8000 times and

infinity times the original lives, respectively, with these bolt removal strategies. The tests completed in this research indicated that these simplistic estimates are generous, because the actual connection stiffness is more complex than suggested by the model and quite variable, as shown by the scatter in Figure 30.

The connection stiffness of the prototype stringer-to-floorbeam connection could not be accurately simulated in the laboratory stringer-to-wall connections because of the variability noted and differences between the prototype connection and the test specimens. However, the change in stiffness for the test specimens was computed, and the changes are shown as $k_s/k_{s,initial}$ in Table 5. These values are different from those calculated with equations 15 and 16. Reasons for this include the approximate way that the values in the table were obtained, increased stiffness due to friction in the connection, and the possibility of loose bolts decreasing the stiffness. Therefore, equations 15 and 16 should be used conservatively. That is, the engineer should work toward greater connection flexibility where possible, rather than using a marginally acceptable reduction in stiffness.

If bolt removal is to be used, care must be taken to ensure that the shear force can be safely carried. The shear force capacity is reduced by the bolt removal DLM, but adequate shear capacity can be assured by one of two methods.

1. The remaining rivets can be replaced by high strength bolts, since the capacity of high strength bolts in double shear is much larger than the design shear capacity of rivets.
1. If high strength bolts are inadequate, additional shear resistance can be achieved by providing an additional seat support beneath the stringer. This is somewhat analogous to the detail shown in Figure 2b, but the web rivets may be retained since the connection is not a movable joint.

Reduction of k_s also means that the end rotation, θ, and deflection of the stringer will be a bit larger under the applied load. It is also necessary to ensure that the movements in the deck caused by the rotations at the ends of the members are not too large. However, recall that the original design of the stringer probably assumed the stringer-to-floorbeam connections were pinned joints, and so these increased deflections should be no larger than intended in the original design. Nevertheless, the increased connection rotations and stringer deflections raise the possibility of increased deterioration and damage to the bridge deck. For the same stringer end rotation, larger deformations will occur at the deck if the top bolts are removed than if the bottom bolts are removed. However, removal of the top bolts should provide a greater reduction in the effective stress in the cope area.

Equation 15 indicates that the connection stiffness can be predicted for a specified bolt group. However, the estimated stiffness may be conservative for bridge stringers in which the cleat is connected to a torsionally flexible floorbeam. If a stringer similar to that being studied is connected to the far side of a floor beam that is flexible in torsion, then moment distribution (assuming that all floorbeams stay at the same elevation) shows that the net stiffness of the connection and framing members is one half of that given in equation 16. That is, for stringers connecting to a floorbeam from one side only,

$$k_s = (275 \times 10^6 \text{ kNm}^3/\text{radian})\, I_{bg} \qquad \text{(Eq. 17)}$$

EFFECTIVE LOAD ON THE STRINGER, P_{eff}

The effective stress, σ_{eff}, determines the number of cycles that a given connection can tolerate, and it establishes the effectiveness of various DLMs. As noted earlier, this stress depends upon the M_{cope}, and M_{cope} depends upon the spring stiffness of the connection, k_s, and the applied load, P. The load on the stringer is a dynamic load applied by trucks and is highly variable. The resulting variability in the stress at the cope is included in the effective stress calculation provided in Equation 2. The variability in

loading is expressed as an effective load, P_{eff}. The stress for a given load varies linearly with the bending moment at the cope, and M_{cope} varies linearly with P. Therefore, the σ_{eff} varies linearly with P_{eff}. Therefore, P_{eff} can be calculated by

$$P_{eff} = \sqrt[3]{\frac{\Sigma n_i P_i^3}{N}} \qquad \text{(Eq. 18a)}$$

where

$$\sigma_{eff} = \frac{M_{cope\ as\ function\ of\ P_{eff}}}{S} \qquad \text{(Eq. 18b)}$$

The variation in load is included in Equation 18, and a measure of the variation is needed to accomplish a rational fatigue evaluation of these riveted, coped stringer-to-floorbeam connections. The loads that induce significant bending moment in a stringer are loads caused by axles or axle groups on individual trucks. This occurs because the maximum moment is developed when the load is near the middle of the stringer span, and little or no moment develops at the cope when the axle is on adjacent spans or near the floorbeams. The load caused by individual axles or two or three tandem axles contributes to P_{eff} because stringer spans are too short to be influenced by total vehicle weight. The dynamic amplification due to impact contributes to this load. It is necessary to consider this variation in dynamic axle loads, and recent research [Roeder et al 1998] on two bridges provides a method for accomplishing this.

Figure 31 is a histogram of the axle loads measured from the right hand lane stringers of the Lewis River Bridge, and this histogram can be used to provide the integration necessary to establish P_{eff} in Equation 18a. It should be recognized that light axle groups contribute little to the effective stress and can be neglected from the effective load (and effective stress) calculations. Therefore, lighter axle groups can be neglected from the evaluations because they have little effect on the resulting fatigue life, and the number count would not be accurate for these smaller loads anyway. In this report, axle

weights of less than 50 kN (11 kip) are ignored for this reason. Also note that an individual truck may contribute more than one cycle because of the multiple axles of many heavy trucks.

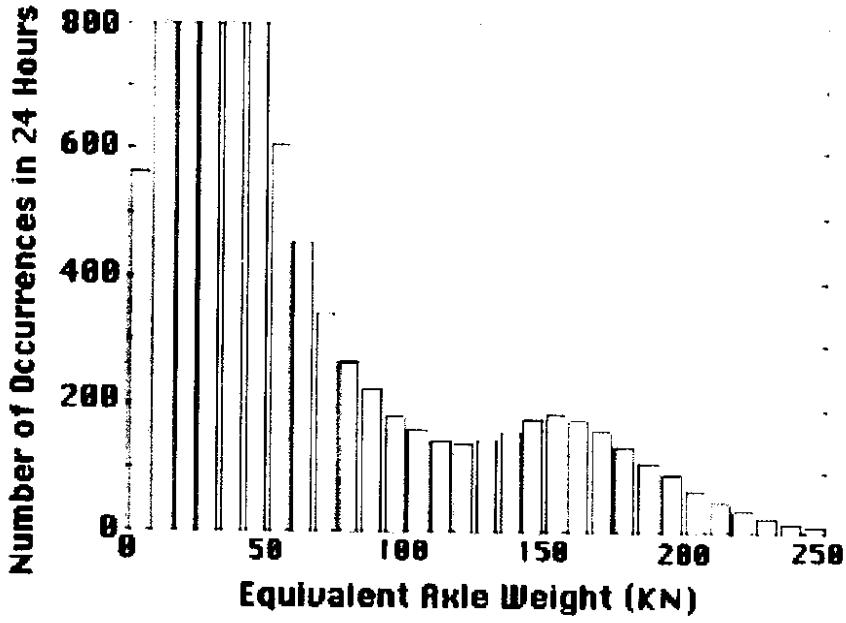

Figure 31. Histogram of Axle Load Variation Measured on the Lewis River Bridge

Similar axle load data were developed for the Toutle River Bridge, and these data are shown in Figure 32. These two histograms look different. However, the difference is misleading because they would both fall at similar positions relative to the S-N curves. The difference in histograms is a result of the trigger point used for the bridges in past studies. Both studies triggered their data acquisition to avoid many thousands of small or lightly loaded trucks, and these triggers were independent and slightly different. A larger number of the lighter trucks are included in the Toutle data, and this leads to the lower P_{eff} value with the larger number of cycles in the Lewis data. Fatigue evaluation with these two separate values will not lead to identical results, but they should lead to very similar results. This variability is appropriate because despite the measurement data, there is still uncertainty regarding the load history of individual bridges.

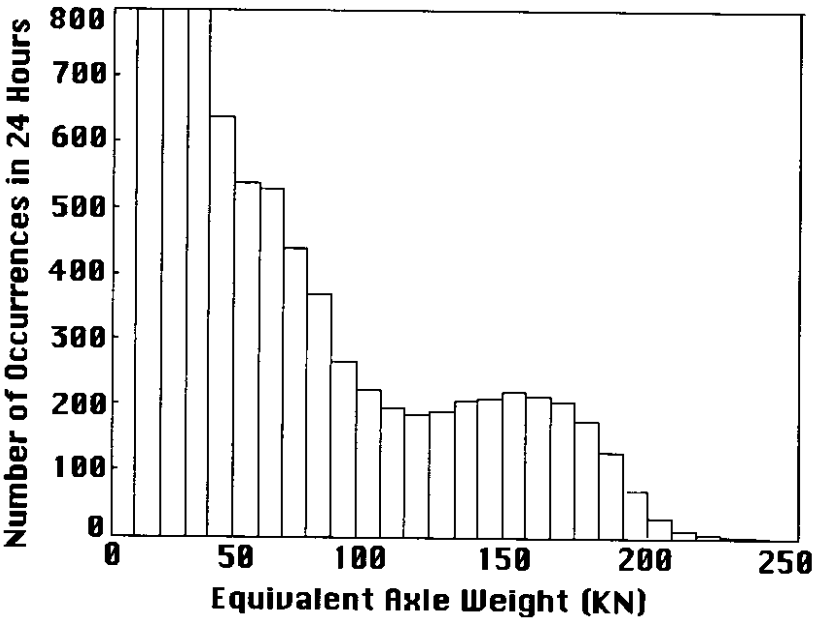

Figure 32. Histogram of Axle Load Variation Measured on the Toutle River Bridge

The P_{eff} values developed from the field measurements are the static axle group loads on the right hand lane of the southbound lanes of Interstate Route 5. Where appropriate this load can now be increased for impact for the specific bridge and can be applied to the individual stringer for calculation of σ_{eff}. However, the full axle load should not be applied to an individual stringer, since this load may be distributed to multiple stringers as shown in Figure 33. Heavily loaded truck axles normally have dual wheels, and usually the outside of the outer wheels is approximately 2.4 m (8 ft) apart, as shown in the Figure 33. Therefore, the loads for individual wheel groups should have a centroidal spacing of approximate 1.8 m (6 ft), as depicted in Figure 33. The actual load that is felt by a stringer depends upon equilibrium and the stiffness of the deck and any transverse stringer diaphragms. However, it is conservative to say that the effective load applied to any individual stringer, $P_{eff\ stringer}$, is the larger of

$$P_{eff\ stringer} = \frac{1.8\ P_{eff}}{2\ S_s} \qquad \text{(Eq. 19a)}$$

or because an individual wheel group may be directly over the stringer

$$P_{\text{eff stringer}} = \frac{P_{\text{eff}}}{2} \qquad \text{(Eq. 19b)}$$

This estimate is conservative in that it neglects the effect of deck stiffness in distributing stringer loads to adjacent stringers.

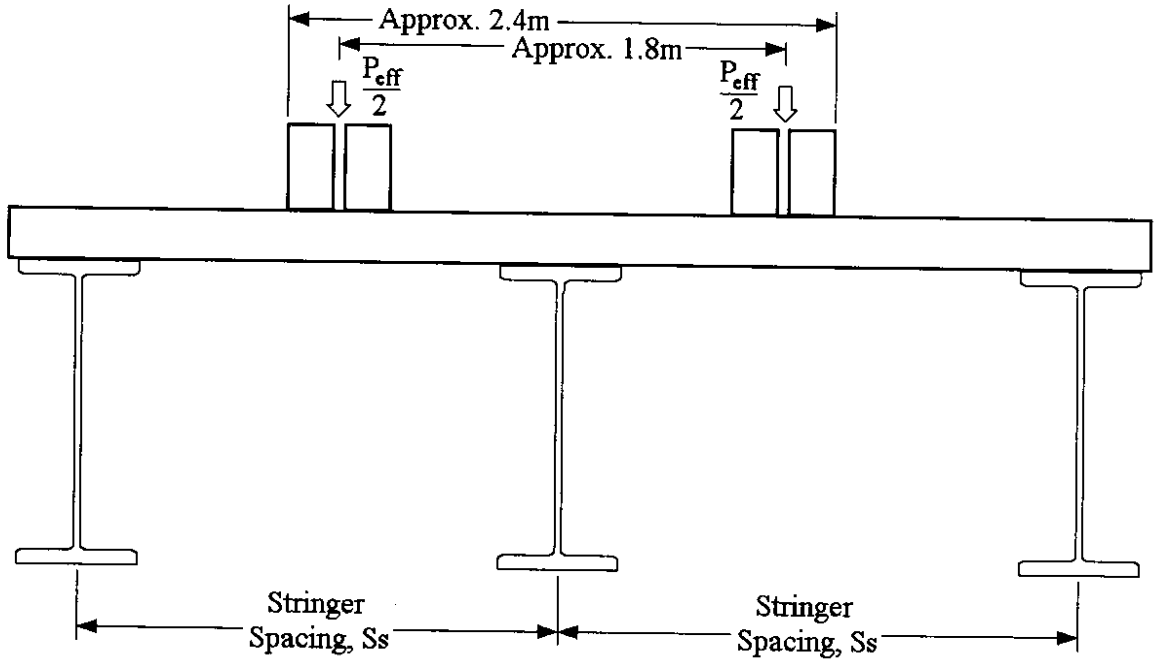

Figure 33. Distribution of Axle Load to Stringers

PROCEDURE TO ASSESS FATIGUE DEMANDS ON AN ACTUAL BRIDGE

The findings in this report can be used to develop a procedure to estimate the time required for fatigue crack initiation, as well as for the expected extension of fatigue life due to the application of different DLMs. The steps and assumptions, as well as an example estimation for the Lewis River bridge, are given below.

Step 1. Obtain the Daily Axle Load Histogram for the Bridge Under Consideration

An axle load histogram for the Lewis River Bridge is shown in Figure 31. This histogram was obtained by the following steps. First, the relationship between actual truck maximum axle weight and stringer response was determined. This was calculated

by first obtaining the maximum static axle weights of a number of trucks at a weigh station, and then by measuring the dynamic stringer response from each of these trucks. A best fit line was made to determine an equivalent static axle weight vs. stringer dynamic response relationship. Once the relationship was established, it was used to relate dynamic stringer response to equivalent static axle weight for vehicles travelling over the bridge in ordinary traffic during several weeks in 1996. The static axle load histogram could be found by plotting the number of times an axle load occurred within each weight range over the period of testing.

It is usually impractical to establish this histogram for every bridge that is analyzed. Therefore, the number of axle loads in each weight range in the histogram for the Lewis River bridge should be scaled by the ratio of the total daily traffic volumes for the subject bridge to the Lewis River bridge at the time of testing. This is suggested because vehicle count data are more likely to be available for less heavily used bridges. The scaling method assumes that the traffic distribution on the bridge under consideration is identical to that on Lewis River bridge. Obviously, this will not be correct for some bridges. However, it is a simple estimate that should be appropriate for an approximate determination of the fatigue life until better data on the truck traffic are available for many bridges.

Step 2. Estimate the Effective Axle Group Force, P_{eff}, and the Number of Daily Loadings, N_{day}

The histogram of Step 1 can then be modified to determine the daily equivalent static axle load. The effective axle group force, P_{eff}, and the number of load cycles per day, N_{day}, may be estimated from a summation or integration of the Daily Axial Load Histogram by using Equation 18a for the year that the histogram data were obtained. This equation assumes that Miners law holds and that the demand is related to the stress cubed.

Dynamic effects must also be considered because the actual load applied by an axle weight in normal traffic will be dynamic. This dynamic force may be estimated by multiplying P_{ef} by an impact factor, IF, to estimate the equivalent dynamic axle load. Impact factors are never precisely determined, but AASHTO provides an equation for estimating this value. AASHTO uses the following equation:

$$IF = 1 + \frac{50}{L + 125} \leq 1.30 \qquad \text{(Eq. 20)}$$

where L is the span length in units of feet. For the Lewis River Bridge, in which the stringer span length was 8.166m = 26.8ft, the impact factor is 1.30. Other methods of estimating IF are available in other specifications. Since the histograms given in figures 31 and 32 were made by correlating dynamic member response and applied static load, P_{eff} determined from the histogram should be multiplied by IF to determine the equivalent dynamic load.

Step 3. Obtain the Relationship Between the Cumulative Number of Axle Loadings and Time

Since the number of trucks on a bridge in any year changes over the years, this effect should be considered in establishing fatigue life estimates. For the Lewis River bridge, plots of the total vehicular traffic versus time were available [Roeder et al 1998]. This graph, which has been extrapolated back to 1950 and up to 2050, is shown as Figure 34. Extrapolation was carried out by using linear approximations from the 1990-1995 data and the 1970-1975 data. If better information is available it should be used.

A relationship of the cumulative number of heavy axle loadings versus time, such as that for the Lewis River bridge shown in Figure 35, should also be obtained. This relationship can be estimated by first dividing the load magnitudes (in Figure 34) by the total amount of traffic (in 1996, 52,000 vehicles) and then multiplying the result by the number of daily heavy axle loadings, N_{day}, in 1996 obtained from Step 2. For the Lewis River bridge, N_{day} is 4702 for equivalent static axle loads greater than 12 kips (53.4 kN).

Second, the equivalent number of heavy axle loadings for any year is found by multiplying the daily value by 365.25. The cumulative yearly equivalent number of heavy axle loadings is then obtained by summing the equivalent yearly number of heavy axle loadings over the years. A start date of 1950 was used because this is when Lewis River bridge construction was completed. Again, this scaling is an approximation, but it should provide an approximate estimate for bridges without extensive truck traffic volume data.

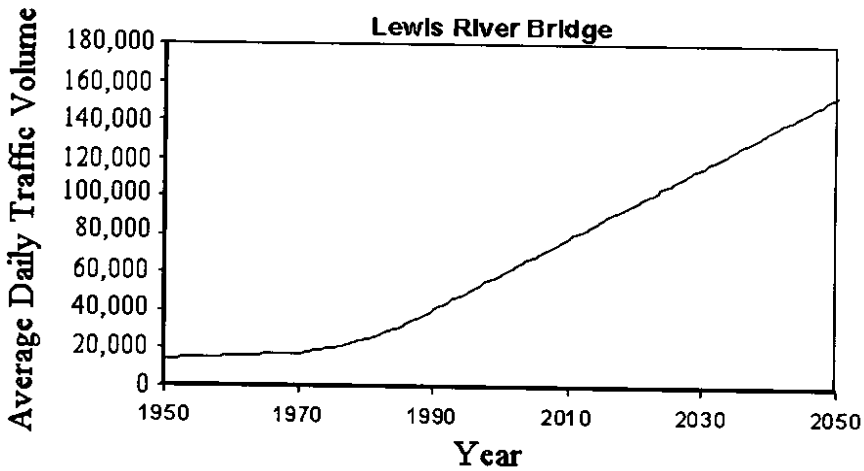

Figure 34. Total Vehicular Traffic vs. Time – Lewis River Bridge

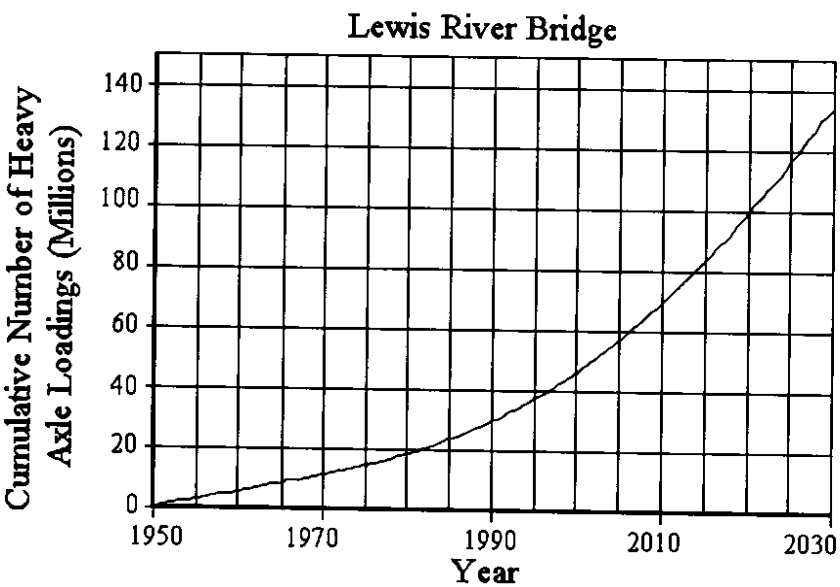

Figure 35. Cumulative Number of Heavy Axle Loadings vs. Time

Step 4. Estimate the Nominal Cope Stress, σ_{cope}

The nominal cope stress, σ_{cope}, is obtained from the dynamic effective axle load, P_{eff}. First, the effective axle load is transformed into an effective group force on a stringer, $P_{eff,stringer}$, by methods illustrated in Figure 33 and Equation 19. Then the second moment of area of the bolt group, I_{bg}, is found from Equation 15 as a function of the bolt size and spacing, and interior stringer end rotational stiffness, k_s, is computed by Equation 17. The interior stringers are expected to be more critical than the exterior stringers because of the low torsional stiffnesses of the floorbeams. The cope moment, M_{cope}, due to $P_{eff,stringer}$ is found by using Equation 14. The elastic modulus of the coped section, S, and the neutral axis depth, c, may be computed from the stringer properties and the cope depth according to the equations in Figure 28, and then the effective nominal cope stress, σ_{cope}, is obtained with Equation 18b.

Step 5. Estimate Initial Cracking

For flame cut copes without notches or corners, on average visible crack initiation may be expected at the number of cycles predicted by Category D with the effective nominal cope stress provided from Step 4. On average, flame cut copes with notches or sharp corners will have visible cracking well before Category E'. The number of cycles for this effective stress level can be translated to remaining years of fatigue life by methods described in Steps 1 through 3.

Step 6. Estimate the Initial Crack Growth Rate

For the test beams, Equation 12 represented a lower bound estimate of the number of cycles for a crack to grow from its size at initiation to a length of 50 mm. Since the beam was at 90 percent scale, the 50 mm length is equivalent to 50 mm/0.9 = 56 mm in the prototype.

Step 7. Estimate the Increase in Life due to the Application of the Hole Drilling DLM

This method slowed crack growth to a rate of approximately 2/3 that predicted by Equation 12. Thus the remaining fatigue life for this method will be approximately 150 percent that predicted for the crack growth rate in Step 6.

Step 8. Estimate the Increase in Life due to the Hole Drilling and Bolting DLM

All specimens in which this method was applied behaved significantly better than Category E after the repair, given the nominal stress. Therefore, Category E can be regarded as a lower bound estimate for the remaining fatigue life, and an average of Category D and E may provide a mean estimate of this remaining life.

Step 9. Estimate the Increase in Life due to the Bolt Removal DLM

Bolt removal causes a decrease in the end stiffness, k_s. The stiffness should be recomputed for the modified connection, and the time period required for further crack growth can be computed by methods described in steps 4 and 6. As noted earlier, a rational goal with this method should be to decrease the moment at the cope to 0.0 because this should prevent tensile stress in the critical region of the cope and provide a maximum extension to the fatigue life. This can be done by reducing k_s so that

$$k_s \leq \frac{\frac{2EI}{L}}{\frac{L}{4L_{cope}} - 1} \qquad \text{(Eq. 20)}$$

It may be necessary to remove more bolts than that indicated by Equation 20 to restrict the likelihood of further crack initiation for the following reasons. First, the decrease in connection stiffness for stringers tested is not as low as that predicted by Equation 16. Second, while the moment is assessed at the corner of the cope, many cracks may initiate and grow at a location closer to the bolt group where the moment is greater. Third, for larger cracks, the method proposed is not likely to be conservative, so extra precautions should be taken.

Remember that provision should be made to safely carry the stringer shear force with this DLM, and larger beam rotations are likely to occur with this method.

EXAMPLE APPLICATION OF THESE CONCEPTS

The procedure above is applied to the stringers of the Lewis River bridge [Skare 1999] to illustrate the likely initiation, crack growth rate, and the differences between various DLMs. The stringers were WF24x76, with a length of 8.166 m spaced at 1.777 m (Skare 1999). For a WF24x76 member, the properties are as follows: t_f = 17.32 mm, b_f = 228.2 mm, d = 607.3 mm, t_w = 11.2 mm, I = 874.1x10^6 mm^4. Cope details are given in Figure 36. The depth of steel at the coped section is d_c = 607.3 mm – 95.2 = 512.1 mm.

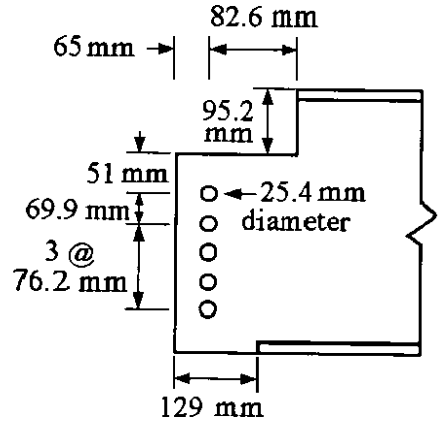

Figure 36. Lewis River Bridge Stringer Detail

Step 1. Obtain the Daily Axle Load Histogram for the Bridge Under Consideration

Since we are dealing with the Lewis River bridge, we can directly use the histogram in Figure 31, which was developed for that bridge. This histogram was developed in 1996 and is for 52,000 trucks/day. If the bridge were different, say N trucks/day, we would then scale the number of trucks at any load magnitude by N/52,000.

The impact factor, IF, for the span length of 8.166 m = 26.8 ft, is 1.3, as provided by Equation 20.

Step 2. Estimate the Effective Axle Group Force, P_{eff}, and the Number of Daily Loadings, N_{day}

The effective axle group force, P_{eff}, and N_{day} were computed by using Figure 31, the impact factor, *IF*, and Equation 18a as follows:

$$P_{eff} = IF.\sqrt[3]{\frac{\Sigma P_i^{\,3} n_i}{N}}$$

$$P_{eff} = 1.3\sqrt[3]{\frac{(58\text{ kN})^3 * 600 + (67\text{ kN})^3 \text{ x } 460 + \ldots\ldots + (263\text{ kN})^3 \text{ x } 10}{4702}}$$

$$= 210\text{kN}$$

Step 3. Obtain the Relationship Between the Cumulative Number of Axle Loadings and Time

For the Lewis River bridge, the relationship in Figure 35 may be used. For other bridges, it should be computed using the method described previously.

Step 4. Estimate the Nominal Cope Stress, σ_{cope}

The effective axle group force on a stringer, $P_{eff,stringer}$, is computed using Equation 19 as follows:

$$P_{eff,stringer} = \max\begin{Bmatrix} \frac{1.8P_{eff}}{2S_s} \\ \frac{P_{eff}}{2} \end{Bmatrix} = \max\begin{Bmatrix} \frac{1.8x210kN}{2x1.777m} \\ \frac{210kN}{2} \end{Bmatrix} = \max\begin{Bmatrix} 106kN \\ 105kN \end{Bmatrix} = 106kN$$

The second moment of area of the bolt group, I_{bg}, is found from Equation 15 for the bolt group shown in Figure 34 as follows:

$$I_{bg} = A_{bolt}\Sigma(r\text{-}r_{centroid})^2 = A_{bolt}\Sigma(r\text{-}0)^2$$

$$= 507\text{mm}^2(76.2^2 + 76.2^2 + (2 \text{ x } 76.2)^2 + (2 \text{ x } 76.2)^2)$$

$$= 29{,}438{,}651\text{mm}^4$$

The end rotational stiffness, k_s, is given by Equation 17 as follows:

$$k_s = (275\text{x}10^6\text{kN/m}^3\text{/radian})I_{bg}$$

$$= (275\text{x}10^6\text{kN/m}^3\text{/radian}) \text{ x } 29{,}438{,}651\text{x}10^{-12}\text{m}^4$$

$$= 8095 \text{ kNm/radian}$$

The cope moment, M_{cope}, due to the effective applied load, $P_{eff,stringer}$, is approximated by using Equation 14 as follows:

$$M_{cope} = P\left\{ \frac{L^2}{8\left(L + \frac{2EI}{k_s}\right)} - \frac{L_{cope}}{2} \right\}$$

$$M_{cope} = 106 \text{ kN}\left\{ \frac{8166^2}{8\left(8166 + \frac{2*200*874.1*10^6}{8095000}\right)} - \frac{86.2}{2} \right\}$$

$$= 0.1192\text{m x } 106\text{kN} = 12.6 \text{ kNm}$$

Using the equations on Figure 28, c = 354 mm and S = 746,642 mm^3. The cope stress, σ_{cope}, is given by Equation 18b, and it is 16.9 MPa.

$$\sigma_{cope} = \frac{M_{cope}}{S} = \frac{12.6kNm}{746{,}642\text{mm}^3} = 16.9MPa$$

Step 5. Estimate Initial Cracking

For flame cut copes in actual bridges there may be severe discontinuities. In this case Category E' is an upper bound on the expected fatigue life. Using Category E' and extrapolating in Figure 24 with σ_{cope} = 16.9 MPa, the upper bound for initiation is at 22,000,000 cycles. Using Figure 35, initiation is expected around the year 1985. This is 35 years after the bridge was constructed. The fact that no cracking was observed in the

Lewis River bridge until after 1992 (Wong, 1997) indicates that the actual cope details in the Lewis River bridge were not as critical as the notched members tested.

Step 6. Estimate the Initial Crack Growth Rate

Given Equation 12, the crack would be expected to grow to a length of 56 mm after N cycles, where

$$N = \frac{5.4x10^{10}}{\sigma_{cope}^{3}} = \frac{5.4x10^{10}}{(16.9\text{MPa})^{3}} = 11{,}185{,}000 cycles$$

If cracking initiated in 1995, when the cumulative number of loading cycles was about 37 million, then 56 mm might be reached after an additional 11.1 million loading cycles, or a total of 48 million loadings. This would be in about 2001, approximately six years after crack initiation.

Step 7. Estimate the Increase in Life due to the Application of the Hole Drilling DLM

If a 25.4-mm diameter hole is drilled 6 mm below a crack tip that is 25.4 mm long, then the distance from the crack tip to the far side of the hole is approximately 6 mm + 25.4mm/2 = 18mm. The expected amount of time that the crack would need to travel 56 mm is 6 years according to Step 10, so the time to crack 18 mm is approximately 18 mm x 6 years/56 mm = 1.9 years if there were no repair. Since the hole extended the crack life by approximately 1.5 times, cracking would be expected to initiate from the far side of the hole approximately 1.5x1.9 = 2.9 years. The increase in time would 2.9 years – 1.9 years = 1.0 year.

Step 8. Estimate the Increase in Life due to the Hole Drilling and Bolting DLM

Based on category E and σ_{cope} = 16.9 MP_a, cracking could reinitiate after 65 million cycles. If the hole was drilled and bolted in the year 2000, cracking initiation from the bolted hole would not be expected until 2023 according to Figure 35. However, it is possible than another crack could start sooner from another location before this time.

Step 9. Estimate the Increase in Life due to the Bolt Removal DLM

If one bolt was removed, the rotational stiffness would decrease to 4,047 kNm/radian according to Equation 17. The cope moment, M_{cope}, due to the effective applied load, P_{eff}, is approximated by using Equation 14 as follows:

$$M_{cope} = P \left\{ \frac{L^2}{8\left(L + \frac{2EI}{k_s}\right)} - \frac{L_{cope}}{2} \right\}$$

$$M_{cope} = 106\ kN \left\{ \frac{8166^2}{8\left(8166 + \frac{2*200*874.1*10^6}{4047000}\right)} - \frac{86.2}{2} \right\}$$

$$\sigma_{cope} = \frac{M_{cope}}{S} = \frac{9.55kNm}{746{,}642mm^3} = 12.79MPa$$

The cope stress, σ_{cope}, given by Equation 18b is 12.79 MPa. Using Equation 12, the crack would be expected to grow a length of 56 mm after N cycles, where

$$N = \frac{5.4x10^{10}}{\sigma_{cope}^{3}} = \frac{5.4x10^{10}}{(12.8MPa)^3} = 25{,}800{,}000cycles$$

If this DLM were applied in 2000, then the stringer should be useable until 2012. Similarly, if two bolts were removed, the time required for crack growth could also be computed.

Another approach to determining how many bolts should be removed is to use Equation 14. Given this equation, the moment at the cope will be 0.0 when

$$k_s < \frac{\frac{2EI}{L}}{\frac{L}{4L_{cope}} - 1} = 1{,}887\ kNm/radian$$

Since this stiffness is 0.233 times the actual stiffness, k_s, of 8095 kNm/radian, the connection stiffness should be reduced to 0.233 times its present value. Removal of two bolts would theoretically decrease the stiffness to 20 percent of its initial value. However, it may be necessary to remove three bolts to restrict the likelihood of further crack growth because of the uncertainties associated with the method.

SUMMARY AND CONCLUSIONS

SUMMARY

This research considered fatigue cracking of the riveted, coped stringer-to-floorbeam connections that are commonly found in truss bridges in Washington State. The work supplemented an earlier field study [Roeder et al 1998] that examined the load spectrum and general performance of these riveted bridges. This earlier work showed that the fatigue cracking is caused by the stress induced by negative bending moments resulting from the rotational restraint or spring stiffness of the connection. The goals of this subsequent study were to replicate the cracking noted in the actual structures, to better understand the causes and rate of crack growth, and to evaluate damage limitation methods (DLMs) for the coped stringer connection.

Sixteen fatigue tests of steel beams with coped stringer connections were completed. Each specimen was initially tested to develop initial cracking. Most of the cracked specimens were modified with a DLM, and they were then tested further to evaluate the effectiveness of the DLM. Three DLMs—drilled hole, drilled hole with inserted bolt, and bolt removal—were considered. The effectiveness of the various DLMs was evaluated and compared. Methods for estimating the remaining life of these damaged bridges and the effectiveness of various DLMs are proposed.

CONCLUSIONS

A number of conclusions can be drawn from this research. Some of the more important conclusions include the following:

- The initial surface condition of a coped region influences the location of initial cracking and the rate of crack growth. Copes with rough or notched surfaces tend to experience fewer cycles until visible cracking initiates, and initial visible

cracking occurs at S-N curves well below AASHTO Category E' for these connections. Flame cut copes without notches and with a surface finish of 250ST or better tolerate a much larger number of cycles until initial cracking. For these specimens, initiation of visible cracking occurs at S-N curves between Category C and E, with Category D being a reasonable mean estimate. Once a visible crack has initiated, the rate of crack growth is no longer dependent on the surface finish.

- The connection stiffness at the end of the stringer has a large effect on the cope stress and the crack growth rate. Stiffer connections result in larger negative bending moments in the cope, larger tensile stress in the cope region, earlier initiation of fatigue cracks, and more rapid crack growth.
- The drilled hole DLM extended fatigue life a short time, but this DLM is relatively ineffective at stopping crack growth. This DLM is far less effective at retarding crack initiation than having a new cope with a good surface finish.
- The drilled hole with inserted bolt DLM is significantly more effective at retarding crack growth than the drilled hole DLM. The drilled hole with inserted bolt may delay crack growth for a long period of time, but it does not change the stiffness of the connection, and so another crack may rapidly develop at an adjacent (but slightly less critical) location. Furthermore, another crack may develop out of the drilled hole (with the bolt in place), and this crack may propagate more quickly than other cracks after this delayed development.
- Washers should be used under the nut and the head of the bolt in the drilled hole with inserted bolt DLM. The washers crack before further cracking of the drilled hole, and therefore, the washers warn of impending crack growth.
- The bolt removal DLM is very effective at retarding crack growth if the resulting connection stiffness is low enough. For optimal performance, the reduction in stiffness should be large enough to reduce the effective bending stress in the

region of the cope to 0.0 or to cause a reversal of the moment to assure that the coped region is in compression during the cyclic loading. If this is not achieved, continued crack growth must be expected, but this growth rate may be significantly slowed if the connection stiffness is reduced to less than 40 percent of its initial value.

- The stiffness of the bolt web connection, k_s, was evaluated, and a linear relationship was suggested for use in quantifying connection stiffness, given the moment of inertia of the bolt group, I_{bg}.
- An evaluation procedure was proposed for evaluating DLMs. This procedure requires estimation of an effective axle load, P_{eff}, and a number of applications of this effective load from the bridge load spectrum. This load is translated into an effective load on the stringers through application of the impact factor and consideration of the distribution of loads between stringers. The previously discussed models of k_s are then used to determine the moment at the cope and the effective stress at the cope location. Equations developed to estimate the number of cycles likely to extend crack growth and various S-N curves are then used to estimate the remaining fatigue life.

RECOMMENDATIONS

This research provided interesting and valuable results. However, considerable room remains for improving the knowledge and understanding regarding this fatigue cracking issue. Several issues of importance are as follows:

- The rate of crack growth is an important issue of concern for the coped stringer connection and the DLMs applied to these connections, but the theoretical basis for evaluating this crack growth is incomplete. Existing linear crack propagation models do not simulate the observed behavior well because they do not

adequately consider the full complexity of the stress distribution of the connection. Further improvements in these models are needed.

- The load spectrum used in the evaluations of these coped stringer connections are based upon field measurements on two bridges in Washington State. These bridges are on Interstate Route 5 and experience very heavy truck traffic. This traffic is not representative of many other bridges in the state. Therefore, methods of developing more general load spectra and translating these spectra into stringer loads are needed.
- This work developed a general hierarchy regarding the effectiveness of several DLMs. Further work is needed to fully understand the rate of crack initiation and growth, both from original coped connections and connections with DLMs.
- The rotational spring stiffness of the connection is a key element in evaluating these coped stringer connections. Limited research has been done on this connection stiffness issue, and further work could significantly improve this fatigue evaluation process.

REFERENCES

AASHTO, "AASHTO LRFD Bridge Design Specifications", American Association of State Highway and Transportation Officials, 1st Edition, Washington, D.C., 1994.

AASHTO, "Standard Specification For Highway Bridges", American Association of State Highway and Transportation Officials, 10th Edition, Washington, D.C., 1973.

AASHTO, "Guide Specifications for Fatigue Evaluation of Existing Steel Bridges," American Association of State Highway and Transportation Officials, Washington, D.C., 1990.

AISC-LRFD, "Load and Resistance Factor Design," Manual of Steel Construction, American Institute of Steel Construction, 2nd Ed., 1995.

Fisher, J., Frank, K., Hirt, M., and McNamee, B.M, "Effect of Weldments on the fatigue Strength of Steel Beams," NCHRP Report 102. Transportation Research Board, Washington D.C., 1970.

Fisher, J., et al., "Fatigue Behavior of Full-Scale Welded Bridge Attachments," NCHRP Report 227, Transportation Research Board, Washington D.C., 1980.

Fisher, J., Yen, B.T., and Wang, D., "Fatigue and Fracture Evaluation for Rating Riveted Bridges," NCHRP Report 302, Transportation Research Board, Washington, D.C., 1987.

Frost, N.E., Marsh, K.J., and Pook, L.P., "Metal Fatigue," Oxford University Press, Ely House, London, England, 1974.

Kalagoris, A. Y., "Fatigue Cracking and Damage Limitation Methods Applied to Coped Steel Bridge Stringers," a thesis submitted in partial fulfillment of the Master of Science in Civil Engineering Degree, University of Washington, Seattle, WA 2000.

Miner, M.A., "Cumulative Damage in Fatigue," ASME, Journal of Applied Mechanics, Vol 12, 1945.

Moses, F., Schilling, C.S., and Raju, K.S., "Fatigue Evaluation Procedures for Steel Bridges," NCHRP Report 299, Transportation Research Board, Washington, D.C., 1987.

Roeder, C.W., "State of Art Report – Connection Performance", FEMA 355D, Federal Emergency Management Agency, Washington, D.C., 2000.

Roeder, C.W., MacRae, G.A., Arima, K., Crocker, P.N., and Wong, S.D., "Fatigue Cracking of Riveted Steel Tied Arch and Truss Bridges," Report WA-RD447.1, WSDOT, Olympia, WA 1998.

Schilling, C.S., Klippstein, K.H., Barsom, J.M, and Blake, G.T., "Fatigue of Welded Steel Bridge Members Under Variable Amplitude Loadings," NCHRP Report 188, Transportation Research Board, Washington, D.C., 1978.

Skare, A. C., "Fatigue Cracking and Repair of Coped Steel Bridge Stringers," a thesis submitted in partial fulfillment of the Master of Science in Civil Engineering Degree, University of Washington, Seattle, WA 1999.

Wong, Scott, D., "Fatigue Evaluation of the I-5 Lewis River Bridge," a thesis submitted in partial fulfillment of the Master of Science in Civil Engineering Degree, University of Washington, Seattle, WA, 1997.

Yam, M.C.H, and Cheng, J.J.R., "Fatigue Strength of Coped Steel Beams," ASCE, Journal of Structural Engineering, Vol. 115, No. 9, Sept. 1990.

Zwernemann, F.J., West, A.B., and Lim, K.S., "Fatigue Damage to Steel Bridge Diaphragms," Journal of Performance of Constructed Facilities, ASCE, November 1993.